Received: 28 March 2022 | Revised: 30 September 2022 | Accepted: 3 October 2022

DOI: 10.1002/hyp.14731

RESEARCH ARTICLE

WILEY

Hydrological process controls on streamflow variability in a glacierized headwater basin

Caroline Aubry-Wake[1] | Dhiraj Pradhananga[1,2] | John W. Pomeroy[1]

[1]Centre for Hydrology, University of Saskatchewan, Canmore, Alberta, Canada

[2]Department of Meteorology, Tribhuvan University, Kathmandu, Nepal

Correspondence
Caroline Aubry-Wake, Centre for Hydrology, University of Saskatchewan, 116A - 1151 Sidney Street, Canmore, AB T1W 3G1, Canada.
Email: caroline.aubrywake@gmail.com

Funding information
Natural Sciences Engineering and Research Council of Canada; Vanier and Michael Smith Scholarships; Canada Foundation for Innovation; Canada Research Chairs; Canada First Research Excellence Fund; Global Water Futures

Abstract

Mountain glacierized headwaters are currently witnessing a transient shift in their hydrological and glaciological systems in response to rapid climate change. To characterize these changes, a robust understanding of the hydrological processes operating in the basin and their interactions is needed. Such an investigation was undertaken in the Peyto Glacier Research Basin, Canadian Rockies over 32 years (1988–2020). A distributed, physically based, uncalibrated glacier hydrology model was developed using the modular, object-oriented Cold Region Hydrological Modelling Platform to simulate both on and off-glacier high mountain processes and streamflow generation. The hydrological processes that generate streamflow from this alpine basin are characterized by substantial inter-annual variability over the 32 years. Snowmelt runoff always provided the largest fraction of annual streamflow (44% to 89%), with smaller fractional contributions occurring in higher streamflow years. Ice melt runoff provided 10% to 45% of annual streamflow volume, with higher fractions associated with higher flow years. Both rainfall and firn melt runoff contributed less than 13% of annual streamflow. Years with high streamflow were on average 1.43°C warmer than low streamflow years, and higher streamflow years had lower seasonal snow accumulation, earlier snowmelt and higher summer rainfall than years with lower streamflow. Greater ice exposure in warmer, low snowfall (high rainfall) years led to greater streamflow generation. The understanding gained here provides insight into how future climate and increased meteorological variability may impact glacier meltwater contributions to streamflow and downstream water availability as alpine glaciers continue to retreat.

KEYWORDS
Canadian Rockies, cold regions hydrology, CRHM, glacio-hydrological modelling, mountain hydrology, streamflow

1 | INTRODUCTION

Glacierized mountain basins provide water to almost one-third of the world's population (Beniston, 2003), but mountain glaciers are retreating quickly and expected to lose 30%–80% of their volume by the end of the century (Huss et al., 2017). Their retreat is impacting water resources across the globe, as glaciers have a strong influence on their basin hydrological regime due to their capacity to store water on seasonal to decadal time scales (Jansson et al., 2003). By storing water as snow and ice during cold and wet periods, and releasing it in dry and hot periods, glaciers can modulate streamflow variability via a compensatory effect occurring both at a decadal, seasonal and even weekly timescale (Jansson et al., 2003). For instance, Pradhananga and Pomeroy (2022a) found that increasing glacier ice melt

compensated for declining precipitation and snowmelt in two Canadian Rockies glacierized catchments, resulting in increased discharge since the 1960s, showcasing the decadal capacity of the glacier compensation effect. On a weekly timescale, van Tiel et al. (2021) found that glacier and snow melt in glacierized basins with a 5%–15% glacier cover could compensate for precipitation deficits and increased evapotranspiration in the European Alps. Even though a glacier coverage of roughly 40% has been suggested to minimize inter-annual variability (and maximize the glacier compensation effect) (Chen & Ohmura, 1990; Fountain & Tangborn, 1985; Jansson et al., 2003), a recent analysis of streamflow in glacierized basins worldwide was not able to define a universal relationship between glacier coverage and streamflow variability and instead hinted at the range of hydrological processes that can complicate the relationship (van Tiel, Kohn, et al., 2020). Snow and ice melt in glacierized basins can also overcompensate for weather conditions and cause an increase in streamflow variability (van Tiel et al., 2021; van Tiel, Kohn, et al., 2020). In the Canadian Rockies, Hopkinson and Young (1998) showed that glacier meltwater does not always effectively augment streamflow during low flow, dry years. This is in accordance with research showing that during cold years, glacier meltwater can be significantly reduced and induce "glacier melt drought" (Van Loon et al., 2015). For tropical glaciers, glacier meltwater can be the driver of variability in streamflow from hourly to annual timescales (Saberi et al., 2019). These results hint at the complex interactions amongst glacier melt, streamflow generation and seasonal meteorological conditions.

The role alpine glaciers play in modulating inter-annual flow variability is further complicated by their recent and predicted retreat (Hugonnet et al., 2021; Radic & Hock, 2014; Shannon et al., 2019). As currently glaciated mountain headwater basins transition from glacier melt runoff to more rainfall-runoff and snowmelt runoff, they will shift towards a more variable hydrological regimes linked with the decreased capacity of glaciers to provide reliable flow compensation. This shift is already noticeable in the Alps and Pyrenees, where runoff volume is more tightly controlled by seasonal snow accumulation and runoff peaks are associated with snowmelt and the occurrence of large rainfall volumes than with glacier melt (Milner et al., 2017). López-Moreno et al. (2020) have shown that as snowmelt-dominated alpine basins warm, their streamflow regimes decouple from snow hydrology regimes, suggesting a progression from glacier-modulated to seasonal snowpack-modulated to rainfall-modulated hydrological regime. There is increasing interannual variability along this progression as hydrological memory times shorten from glaciers to seasonal snowpacks to rainfall (Milner et al., 2017). Combining this decrease in the interannual buffering capacity of glacier runoff with an expected increase in extreme weather and hydrological events such as increased heavy precipitation and droughts (Seneviratne et al., 2012), significant changes are expected to occur to the hydrology of mountain glacierized headwater basins around the world.

Analysing the influence of glacier runoff on headwater basin streamflow is further complicated by the variety of approaches used to define glacier contributions to streamflow. Within the range of methodologies, glacio-hydrological modelling is the most used (Frenierre & Mark, 2013). Glacio-hydrological models can be used to increase the understanding of the observed processes in a basin (Verbunt et al., 2003), and can help diagnose the relationship between the different hydrological processes. These glacio-hydrological models are typically adapted from models with either a glaciological or hydrological background, depending on the intended use. Glaciological models typically focus on the ice processes, for example, the representation of ice dynamics (Huss et al., 2010; Clarke et al., 2015) or surface mass balance (Hock and Holmgren, 2005), but either ignore or simplify the other hydrological and cryospheric processes (Immerzeel et al., 2010). Hydrological models typically simplify the glacier-specific processes, such as neglecting ice dynamics (Comeau et al., 2009; Jost et al., 2012), but can have more sophisticated representations of the terrestrial hydrological cycle. Both model approaches often use a conceptual approach to parametrize surface melt, using statistical associations to infer mass and energy fluxes, such as the calibrated temperature-index, degree-day and melt models (Hock, 2003; Finger et al., 2011; Fatichi et al., 2014; Ragettli et al., 2016; Chernos et al., 2020). While this makes them easier to apply in areas with incomplete forcing data, a typical issue for mountain environments, it also makes them more prone to problems such as equifinality (Beven, 2006), which can be reduced by using multi-criteria calibration procedures (Hanzer et al., 2016; Jost et al., 2012; Pellicciotti et al., 2012; van Tiel, Stahl, et al., 2020). A further concern with these calibrated empirical modelling approaches is their transferability in time (Hock, 1999), especially their ability to simulate conditions outside of the conditions encountered in the calibration period (Duethmann et al., 2020). Some glacio-hydrological model calibration strategies involve using unusual years, such as the hot and dry year of 2003 in the European Alps, to assess model performance under extreme events (Koboltschnig & Schöner, 2011). However, with rapidly changing meteorological conditions and land cover, past conditions are not likely to represent future melt and hydrological events in glacierized alpine basins. Empirically calibrated glacio-hydrological models also increase predictive uncertainty as they are not consistent with the current understanding of glacio-hydrological physical processes. Since shortwave radiation rather than air temperature is the main driver of glacier melt, and snow redistribution is an important control on snow accumulation, the lack of a physical basis for these models is scientifically unsatisfying in that process diagnoses are not possible and predictive uncertainty is high because they are calibrated to past climate and glacier conditions. Models with a more complete range of representations of glacio-hydrological processes do exist (Frans et al., 2018; Naz et al., 2014; Pradhananga & Pomeroy, 2022b; 2022a), but these are still not widely used despite the uptake of models of similar complexity for cold regions hydrological applications (Wheater et al., 2022). To investigate the inter-annual variability in the hydrology of a glacierized headwater basin and to diagnose the hydrological processes governing this variability requires a physically based model, with representations of both on and off-glacier biophysical processes. Glacierized basins are complex systems, with several hydrological processes on and off the glacier such as snow redistribution, accumulation and ablation, glacier processes, infiltration into seasonally frozen soils,

groundwater storage and flow, frozen ground, evapotranspiration and a dynamic land cover. These interconnected processes, driven by complex physical feedbacks, should be included in hydrological assessments of glacierized headwater basins to gain a robust understanding of the sources of hydrological variability occurring in these basins.

The objective of this paper is to assess and characterize the interannual hydrological variability of a long-studied alpine glacierized headwater basin in the Canadian Rockies using observations and a physically based glacio-hydrological model, including the full range of processes occurring both on and off the glacier. Specifically, this study investigates the influences of meteorological conditions on hydrological processes, meltwater production, runoff and streamflow variability by addressing the following questions:

1. What trends are evident in the hydrometeorological behaviour of the basin in the recent decades?
2. How do runoff source and streamflow regime vary with seasonal hydrometeorological conditions?
3. How do meteorological conditions, snow dynamics and sources of runoff vary between high and low streamflow years?

2 | DATA AND METHODS

2.1 | Study site and available data

This study focused on the Peyto Glacier Research Basin (PGRB, Figure 1), a small glacierized headwater basin in the Canadian Rockies. Peyto Glacier, the northernmost outlet glacier of the Wapta Icefield, ranges between 2100–3190 m.a.s.l. and had an area of 10.2 km^2 in 2016, with a drainage basin of 19.3 km^2 as defined by a stream gauge installed by the University of Saskatchewan's Centre for Hydrology in 2012. Peyto Glacier is one of the few well-monitored glaciers in western Canada, and has one of the longest time series of measurements in the world, with mass balance observed yearly since 1965, and glacier extent measured since 1896 (Demuth et al., 2006). The rest of the basin is composed of moraine deposits, talus fields, and exposed bedrock, including cliffs (Figure 1b).

The meteorological data used for model forcing and evaluation in this study have been described in detail in Pradhananga et al. (2021) and by Pradhananga and Pomeroy (2022b), but a summary is provided here. An automated weather station (AWS), Peyto Main Old, has recorded sub-hourly to hourly air temperature, relative humidity, incoming solar radiation, incoming longwave and wind speed since 1987, at an altitude of 2240 m.a.s.l. Due to the remote location and harsh conditions found in the basin, gaps are present in the data since the installation. The record from Peyto Main Old between 1987 and 2018 is 94% complete, with few gaps in the 2018 to 2020 period. When data gaps were less than or equal to 4 h, they were filled with either linear interpolation, and when gaps were more than 4 h, they were filled with data from nearby stations using monthly linear regression such as from the new Peyto main station, installed in 2013 adjacent to the Peyto Main Old AWS. When nearby stations were not available to fill the missing data, the gaps were infilled using ERA-Interim data, which were bias-corrected and downscaled to the station location using a quantile mapping technique with monthly calibrated parameters from in-situ data (Dee et al., 2011).

Precipitation for the PGRB for 1987–2020 was obtained from the ERA-Interim reanalysis product. The ERA-Interim precipitation

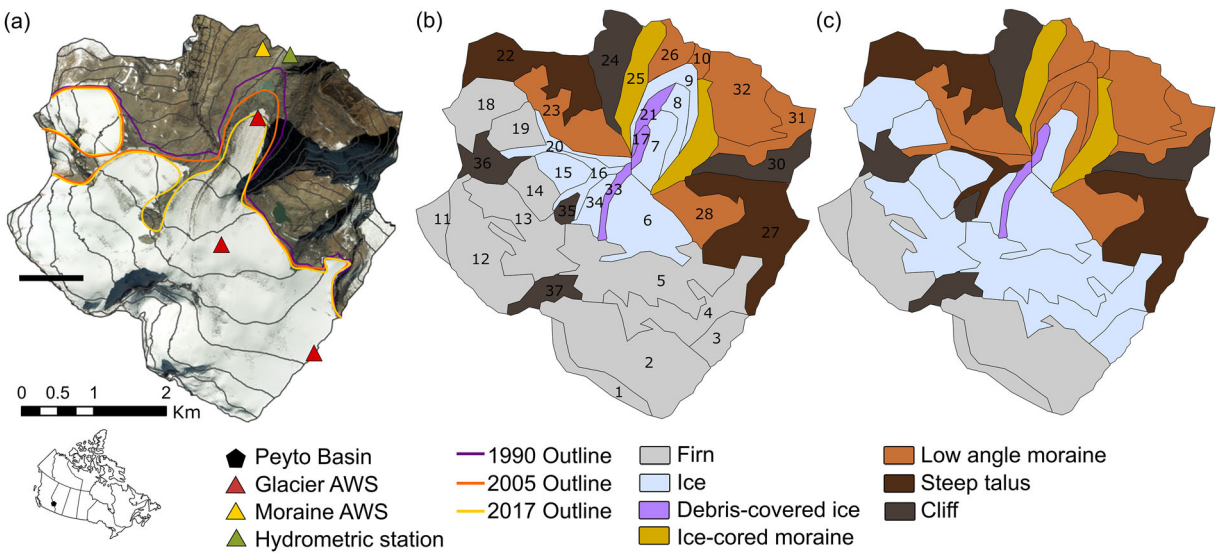

FIGURE 1 Peyto Glacier Research Basin (a) from aerial imagery in 2014. Yellow, red and green triangles indicate locations of the Moraine AWS, Glacier AWS and the Centre for Hydrology hydrometric station. Thin grey lines in (a) are terrain contours at 100 m intervals, from 2100 to 3000 m.a.s.l. The glacier extent, surface cover type and spatial discretization of hydrological response units (HRUs) are shown for (b) 1990 and (c) 2015. The number labels on (b) refer to the Table A1 presenting the geomorphic characteristics of the HRUs. The basin outlet is located at HRU 10.

data were also corrected using the quantile mapping technique using monthly calibrated factors, but the in-situ data used to derive these factors were obtained from the Alberta Environment Bow Summit weather station, located 5 km down valley at an elevation of 2030 m. a.s.l., from which a reliable, sheltered-environment hourly precipitation record is available since 2008.

Glaciological data are available both as elevation-band averaged summer and winter point mass balance for the 1993–1995 period (Dyurgerov, 2002) and as individual stake point-balance measurements for the 2003–2017 years. Additionally, glacier surface elevation change was measured intermittently using an ultrasonic depth sensor on the on-ice AWS for the 2011–2020 period, and surface lowering associated with ice melt has been transformed to surface melt water equivalent using an ice density of 0.9 kg m^{-3} (Benn & Evans, 2010).

In 2013, an ultrasonic depth sensor (SR50) was installed 1 km below the glacier snout at a bedrock constriction, which acts as a natural notch, providing a reliable control on the relation between streamflow and stage discharge Starting in early fall 2017, salt dilution measurements were performed to build a rating curve to relate the water level at the sonic depth sensor to discharge (Pradhananga et al., 2021; Sentlinger et al., 2019). Manual stream width measurements provided values ranging between 8 and 13 m, and a mixing reach of length of 420 m was set based on the local geomorphology to constrain the salt measurement between two naturally occurring bedrock notches constricting the flow. A total of 105 salt dilution measurements were conducted between 2017 and 2019 and processed in the Fathom Scientific Salt Portal platform, an online post-processing platform for salt dilution measurements (salt.fathomscientific.com). Of these 105 measurements, 46 were determined to be anomalous due to incomplete mixing associated with the choice of location for the conductivity probe, localized snowmelt runoff and the high background noise in electrical conductivity. The resulting rating curve, based on 59 measurements with an average uncertainty of 12%, is a power law with an inflection point at depth of 0.75 m due to a change in the slope of the bedrock notch walls. The rating curve is stable over the 2017–2019 observations, as expected from the bedrock notch controls on streamflow over the salt dilution mixing reach. This stability suggests it is appropriate to use the same rating curve for the entire 2013–2020 melt seasons. Streamflow observations are only possible when the melt channel is sufficiently free of snow that the SR50 sensor can measure open water, which results in streamflow measurement available from mid-May/early June to late September/mid-October.

2.2 | Modelling approach

The Cold Regions Hydrological Modelling Platform (CRHM, Pomeroy et al., 2007; Pradhananga & Pomeroy, 2022b) was used to investigate the hydrological processes and inter-annual variability in the PGRB. The model was run at an hourly resolution for the period 1987–2020, with the first year acting as a spin-up period. The modelled period covers 32 continuous hydrological years (October 1st – September 31st), starting in October 1988 and ending in September 2020. The model outputs were aggregated into daily values for the analysis. The analysis period was dictated by the availability of in-situ meteorological information in the PGRB (Pradhananga et al., 2021).

Cold Regions Hydrological Modelling is a process-based, flexible, modular hydrological modelling platform. The user can select processes from an extensive library to assemble a custom hydrological model suited to the complexity, knowledge and available data from the study environment. CRHM has been extensively used in mountains in the recent years (DeBeer & Pomeroy, 2009; Fang et al., 2013; Krogh et al., 2015; López-Moreno et al., 2017; MacDonald et al., 2010; Rasouli et al., 2014; Zhou et al., 2014) with applications over different terrain and climate and at different spatial scales. A glacier module has recently been developed to represent ice and firn melt and mass balance using an energy balance approach (Pradhananga & Pomeroy, 2022b). This model is selected amongst other models because it has spatially distributed energy balance forcing and a set of modules that represent hydrological processes suitable for the PGRB including blowing snow transport and sublimation, complex terrain wind flow, avalanching, infiltration into seasonally frozen soils and evaporation from soils, vegetation and open water and surface and sub-surface runoff generation.

The modelling work presented here used the CRHM model development from Pradhananga and Pomeroy (2022b) and the PGRB data processing of Pradhananga et al. (2021). However, it differed substantially from the CRHM application to the PGRB by Pradhananga and Pomeroy (2022a; 2022b). The study used in-situ forcing data instead of reanalysis data (except precipitation) and simulated different time periods (1989–2020 in this case and 2013–2018 and 1967–1977 in Pradhananga & Pomeroy, 2022a). In addition, the current application used a different energy-balance parametrization for the glacier ice melt at an hourly timestep as described in Section 2.2.2 (Snow and ice melt), whilst Pradhananga and Pomeroy (2022a) used a daily formulation without parametrization of sub-debris melt. The model spatial discretization and parametrization was performed independently from these previous studies and resulted in a different parametrization. For example, Pradhananga and Pomeroy (2022a) had a spatial discretization with 65 HRUs, and only 37 are used in this study. In addition, the research goals of this study, specifically to investigate processes resulting in streamflow variability in the PGRB, were different from those of Pradhananga and Pomeroy (2022a; 2022b), and therefore resulted in a different analysis methodology.

2.2.1 | Spatial discretization

In CRHM, the mass and energy balance are calculated at the scale of hydrological response units (HRUs), a spatial unit over which the mass and energy balance is assumed to be spatially uniform. HRUs are defined as regions with similar hydrological characteristics and common parameters, based on topographic, drainage, vegetation, soils and hydrometeorological properties. Here, glacier properties were also included in discretizing the basin into HRUs. PGRB was divided into

36 HRUs that represent the glacier retreat over the 1987–2017 period, as well as the firn line retreat and major land cover types such as moraine, talus, ice-cored moraine and cliffs (Figure 1b,c). The changing land cover types were manually defined using a combination of Landsat imageries for glacier and firn, and field observations for cliffs, moraines and talus characterization. The ice-cored moraine area was defined following Hopkinson et al. (2012). For each HRU, parameters such as slope, aspect, elevation, and terrain view factor were then defined using the SRTM digital elevation model. The resulting HRUs, with associated cover-type, can be seen in Figure 1b,c, and the elevation, slope, angle aspect and cover-type of each HRU can be found in Table A1.

2.2.2 | Physical processes representation and parametrization in CRHM-glacier

A purpose-built model representing the hydrological processes observed in the PGRB was designed by selecting modules in the CRHM modelling library. Parameters for each module have a physical meaning and can be obtained from field site or remote sensing observations. When parameters specific to the site are unavailable, parameters are obtained following the abduction approach (Pomeroy et al., 2013), meaning they are transferred from studies in similar environments or obtained from compatible hydrological environments described in the scientific literature. In other words, as this CRHM model is based on physical processes, it does not require a parameter calibration scheme based on streamflow observations. The CRHM process representation and parameter estimation approaches are described below.

Distributing meteorological inputs

The CRHM model created for PGRB distributes the forcing meteorology, namely observations of air temperature, relative humidity, wind, incoming shortwave and longwave radiations and wind speed, spatially and temporally over the basin. The air temperature lapse rate was defined for monthly values, ranging from −0.57 to −0.81°C per 100 m, obtained from three on-ice AWS located on the glacier toe, near the equilibrium line, and in the accumulation area for the years 2010–2013 as in Pradhananga and Pomeroy (2022b) (Figure 1a). The shallowest temperature elevation lapse rates (slower decrease in temperature with elevation gain) occurred in July and August, with generally steeper temperature elevation lapse rates (faster decrease in temperature with elevation) occurring in Fall and Spring. Monthly values for the temperature lapse rates were fixed throughout the simulation period (i.e., all Januaries had the same lapse rate). The precipitation elevation gradient was derived from the end-of-winter SWE point measurement over the glacier area for two 3-year periods (2003–2005 and 2014–2016) and so integrates the winter snow accumulation season. The same precipitation gradient was used for all seasons, as there was no information available to estimate a seasonally varying gradient for this basin. Precipitation phase partitioning was calculated using the psychometric energy balance of a falling hydrometeor based on air temperature and relative humidity (Harder & Pomeroy, 2013). Wind flow acceleration and deceleration over PGRB's complex terrain, an important component to capture blowing snow processes and turbulent transfer calculations, were simulated following a linearized turbulence model (Walmsley et al., 1986). Radiation was adjusted for self-shading and slope-aspect following the formulations of Garnier and Ohmura (1970), but it was not corrected for shading from surrounding terrain.

Snow redistribution

Cold Regions Hydrological Modelling simulates winter snow redistribution from blowing snow with the Prairie Blowing Snow Model module (Pomeroy et al., 1993; Pomeroy & Li, 2000), which was initially developed in the Canadian Prairies but has since then been parameterized for alpine and arctic tundra (Pomeroy et al., 1997), mountainous subarctic terrain (MacDonald et al., 2009) and mountain ridges (MacDonald et al., 2010). The blowing snow sequence follows the dominating westerly wind patterns, from the peaks on the continental divide, east to the glacier toe. Blowing snow redistribution requires a terrain roughness specification, which in the absence of vegetation represents surface undulations and barriers. This was set to between 0.5 and 3 m based on cover type and field observations. Fetch distance was obtained from the length of the HRU in the predominating wind direction.

In high mountain environments, avalanches can redistribute an important part of the snow accumulation (Shea et al., 2015). Avalanches are highly dependent on slope, snow accumulation and meteorological factors (Freudiger et al., 2017; Schweizer et al., 2008). CHRM uses the SnowSlide model as a module to represent avalanche redistribution of snow, based on a threshold snow holding depth and slope (Bernhardt et al., 2012; Bernhardt & Schulz, 2010). The minimum threshold depth was set to 500 mm w.e. for most HRU, with a holding capacity of 50 mm w.e. for the HRU with a surface slope angle above 30°, as steep terrain is more likely to avalanche frequently (McClung & Schaerer, 2006).

Snow and ice melt

Snowmelt on- and off-glacier in CRHM is calculated with the SNOBAL module (Marks et al., 1999). This module approximates the snowpack as being composed of two layers: a surface-active layer of fixed thickness and a lower layer representing the remaining snowpack. The module solves for the temperature, liquid water content and the specific mass of each layer for each time step. The point energy balance of the snowpack is expressed as in the following:

$$Q_m = Q^* + Q_H + Q_E + Q_G + Q_P - \frac{dU}{dt} \quad (1)$$

Where Q_m is the energy available for snowmelt, Q^* is the net radiation composed of both shortwave and longwave components, Q_H, Q_E and Q_G are the sensible, latent and ground heat fluxes, respectively, Q_P is the energy added to the snowpack by precipitation, all in W m^{-2}, and U is the internal energy of the snowpack in Joules. The snow albedo

decay function (Essery & Etchevers, 2004) requires a maximum (fresh snow) and a minimum (bare ground) albedo, which in this case was set to 0.85 and 0.17 from regional observations. For glacier and firn, the albedo was set to 0.3 and 0.5 respectively. The snowmelt module was given a surface snow roughness of 0.0055 m based on the observations of Munro (1989) from Peyto Glacier. Turbulent transfer energy fluxes in the module are calculated using a bulk transfer formulation with the Monin-Obukhov stability corrections.

Once the snow is melted, glacier ice melt is calculated using a single layer energy balance model, with the residual of the radiation and turbulent fluxes resulting in energy available for melt (Hock, 2005). The model distinguishes between firn and ice cover for albedo, roughness length and density. The energy balance formulation for the ice and firn melt uses turbulent energy fluxes calculated following the katabatic parametrization of the bulk transfer method as described by Grisogono and Oerlemans (2001) and tested at Peyto Glacier by Munro (2004). This is an advance over the simpler daily ice melt energy balance parameterization employed in CRHM previously by Pradhananga and Pomeroy (2022b; 2022a) in that sub-daily fluxes can have important contributions to seasonal melt. If the snowpack is not completely melted by the end of the summer, the snow becomes firn. Firn densification occurs through a 5-layer system, with density increasing from 450 to 850 kg m^{-3}. The densification rate was set to 100 kg m^{-3} yr^{-1} to be consistent with observations.

Further addition to the CRHM model of PGRB is the inclusion of melt under debris-cover, calculated following the empirical equation of Carenzo et al. (2016). This formulation was shown to have similar results to an energy-balance approach treating the energy transfer as conductive energy flux, driven by the conductivity of the debris layer and the temperature gradient (Reid & Brock, 2010). Ice-cored moraines are another type of debris-covered ice, a common feature in mountain environments (Gruber & Haeberli, 2009; Østrem et al., 1970). In the PGRB, Hopkinson et al. (2012) found that runoff from the periglacial areas accounted for 8% of the water losses from basin storage for the period 2000 to 2010. Debris cover thickness in the PGRB was obtained from multiple point measurements over the study area from ice cliffs and manually digging pits during field site visits. The debris thickness varied from thin debris (5–10 cm thickness) in steep areas and on the edge of the medial moraine, to value of 0.5 m in the main area of the medial moraine. In the debris-covered area on the western side of the glacier toe, the maximum debris thickness measured was of 1.4 m, with an average of 0.53 m (Aubry-Wake et al., 2022).

For each glacier HRU, runoff water (rainfall on glacier area and meltwater) is routed vertically through the snow, firn and ice reservoir to the glacier-rock interface using a linear reservoir approach (Hock & Noetzli, 1997). Each layer (snow, firn and ice), and for each HRU, has its own reservoir with a static value for the duration of the simulation. The snow reservoir of each HRU is connected laterally to other HRUs through blowing snow and avalanching mass fluxes, but the ice and firn reservoirs are not connected laterally to other HRUs as there is no ice dynamics implemented in this model. Due to the fast routing observed in this basin, these storage values are set to zero. Once the ice thickness of a glacier HRU reaches zero, the cover type is automatically converted to bare rock without interrupting the simulation. The elevation of the glacier HRUs evolves following the surface melt or accumulation throughout the simulation. For the glaciers HRUs that melt out during the simulation, the initial ice volume was determined to match the year of glacier retreat based on the glacier outlines for 2005 and 2017 (Figure 1a). For example, the ice thickness in HRU 9, corresponding to the glacier toe, was set to completely melted out by 2005.

Infiltration and subsurface flow and storage

Once the snow and ice meltwater and rainfall runoff reach the glacier-rock interface of individual HRUs, the water is routed through the soil module to produce surface runoff, infiltration and subsurface runoff as per Fang et al. (2013). Similarly, the snowmelt and rainfall runoff from the non-glacierized HRUs, composed of rock debris and exposed bedrock, is also handled by the soil module. Infiltration into unfrozen soils is calculated following Ayers (1959) and into frozen soils following Gray et al. (2001). For unfrozen soil (Ayers, 1959), alpine soil texture parameters were transferred from Marmot Creek Research Basin, further south in the Canadian Rockies (Fang et al., 2013). Frozen and thawed soil moisture initial conditions for storage and moisture content were obtained using a one-year spin-up period (1987).

The soil module is divided into a recharge layer, from which evapotranspiration can occur, a subsurface and a groundwater layer. Each soil layer, for each HRU, has a storage volume and a saturated hydraulic conductivity which dictate the fate of the meltwater and rainfall-runoff for each HRUs: saturation excess water becomes surface runoff routed to another HRU, whilst infiltrated water contributes to subsurface runoff and groundwater flow. Groundwater recharge occurs via percolation from the soil layers and groundwater discharge takes place through horizontal drainage in the groundwater layer. Subsurface discharge occurs via horizontal drainage from either soil layer, with the lateral flow calculated using Darcy's law for unsaturated flow, as described by Fang et al. (2013). Surface runoff forms when melt or rainfall rates exceed the infiltration rate (infiltration excess surface runoff) or when they exceed the subsurface withdrawals from saturated soils (saturation excess surface runoff). The presence of water ponding in surface depressions has been observed in the moraine, the ice-cored moraine and the low angle talus environments. This was represented in the model as a depressional storage capacity set for these HRUs. When depressional storage capacity is present, surface runoff refills this storage before it can contribute to downstream runoff.

The soil module was parametrized based on the cover types in the basin: clean ice, debris-covered ice, steep talus, low angle talus, moraine and cliffs (Table 1). For the clean ice HRUs, the glacier was assumed to be sitting on bedrock with minimal subglacial debris, and therefore, was given low storage volume. For the debris-covered glacier HRUs, the subsurface layer storage was set to a volume varying with debris thickness to represent moisture storage in the debris layer, as the debris-layer does not have a reservoir layer of its own. For the talus and moraine non-glacierized HRUs, the recharge soil layer was set to represent the coarse and shallow surface rock debris, and the subsurface layer was set to represent the thicker underlying moraine

TABLE 1 Subsurface storage and routing parameters (saturated hydraulic conductivity in m d^{-1} and storage in mm)

	Moraine	Low talus	Steep talus	Cliff	Clean ice	Debris cover
Maximum recharge layer storage	1	1	1	1	1	1
Maximum lower layer storage	1050	60	30	1	1	60–150
Maximum groundwater layer storage	1000	1000	1000	1000	1000	1000
Saturated hydraulic conductivity – upper soil layer	0.03	0.03	0.03	0.03	0.03	0.03
Saturated hydraulic conductivity – lower soil layer	0.001	0.01	0.01	6.95×10^{-7}	6.95×10^{-7}	0.001
Saturated hydraulic conductivity – groundwater layer	6.95×10^{-7}	6.95×10^{-7}	6.95×10^{-7}	6.95×10^{-7}	6.95×10^{-7}	6.95×10^{-7}

and talus debris, following field observations. The storage parameters for talus and moraine land cover were based on extensive studies of talus and moraine groundwater flow processes at Lake O'Hara Research Basin in the Canadian Rockies (Hood & Hayashi, 2015; Langston et al., 2011; Mcclymont et al., 2010; Muir et al., 2011). Moraine deposit HRUs were set to have the largest storage capacity, being composed of coarse to fine sediment size. The storage in steep talus slopes (coarse, irregular rocks with large void space) HRUs was set to small values based on Langston et al. (2011), who found talus slopes to have a thin saturated layer (0.01–0.1 m) at the bedrock-talus interface, which quickly transmits water to the downslope environment. This low storage capacity increases for low-angle talus HRUs, where micro-topographies can enhance water storage. Minimal soil storage was assumed for the cliff HRUs, as these are bedrock with limited debris moisture storage. The storage of groundwater layer, set to represent the bedrock storage, was set to the same value across the basin and reflects the porous limestone lithology of basins in the region (Fang et al., 2013).

The saturated hydraulic conductivities for talus and moraine sediments were transferred also from Lake O'Hara (Langston et al., 2011; Mcclymont et al., 2010; Muir et al., 2011). Talus fields studied in the Canadian Rockies had a very high hydraulic conductivity (0.01–0.03 m s^{-1}) (Mcclymont et al., 2010), with similar values obtained by Clow et al. (2003) in a talus and rock-glacier dominated basin in the Colorado Rockies.

Routing

Routing of runoff from the surface and subsurface layers between the HRUs is handled in CRHM by Clark's lag and route algorithm (Clark, 1945; Pomeroy et al., 2007) following a user-specified routing order. This user-defined order means that water in the soil, subsurface and groundwater layer can move laterally between HRUs to simulate the flow of water through the basin, from higher elevation to lower elevation and converging towards to basin outlet. In this implementation of CRHM, no stream channel exists, and the basin outflow was calculated as the water leaving the outlet HRU (HRU 10, Figure 1b). For each HRU, water that infiltrated into the groundwater reservoir was assumed to leave the basin as groundwater flow in a "leaky basin" and was not captured at the basin outlet streamflow, or the simulated streamflow compared to measured streamflow.

The lag and route method translates each HRU's inflow into outflow based on a lag time and a storage constant. Considering the flashiness of the system, with meltwater reaching the outlet of the basin in a few hours to half a day (Munro, 2011; 2013; Ommanney, 2002), the routing through the basin was assumed to occur within a day, the minimum timestep at which the streamflow was analysed. To capture this fast routing, the routing parameters (lag time and storage constant) for snow and ice melt as well as surface and subsurface flow were set to zero. The groundwater reservoir storage constant was set to 10 days for low-angle HRUs and 5 days for steep HRUs based on the physical understanding of alpine groundwater flow and storage (Hayashi, 2020).

2.3 | Assessing model performance

Using multiple lines of evidence to evaluate model performance is critically important to reduce internal inconsistencies and improve model fidelity (Finger et al., 2011; Pellicciotti et al., 2012; Schaefli and Huss, 2011; van Tiel, Stahl, et al., 2020). The model was evaluated using four sets of observations relating to snow accumulation and ablation, glacier melt, and streamflow. Snow accumulation and glacier melt across the glacier area were assessed using point mass balance measurements by the Geological Survey of Canada for the period 2005–2018 (Figure 2a,b). 240-point measurements for winter and 163 for summer mass balance were made using drilled, surveyed stakes between elevation 2136 and 2760 m.a.s.l. For the years 1989–1995, the mean mass balance by elevation band was used to evaluate model performance. The simulated summer and winter mass balance were extracted for the same date as the recorded measurements, generally corresponding to late April or early May for winter mass balance and late September for summer mass balance surveys.

Model evaluation is done with a range of metrics as appropriate for each dataset. The Nash-Sutcliffe efficiency (NSE, Nash and Sutcliffe, 1970) is calculated as follow:

$$\mathrm{NSE} = 1 - \frac{\sum_{t=1}^{t=T} \left(x_{\mathrm{sim}}(t) - x_{\mathrm{obs}}(t)\right)^2}{\sum_{t=1}^{t=T} \left(x_{\mathrm{obs}}(t) - \overline{x_{\mathrm{obs}}}\right)^2} \quad (2)$$

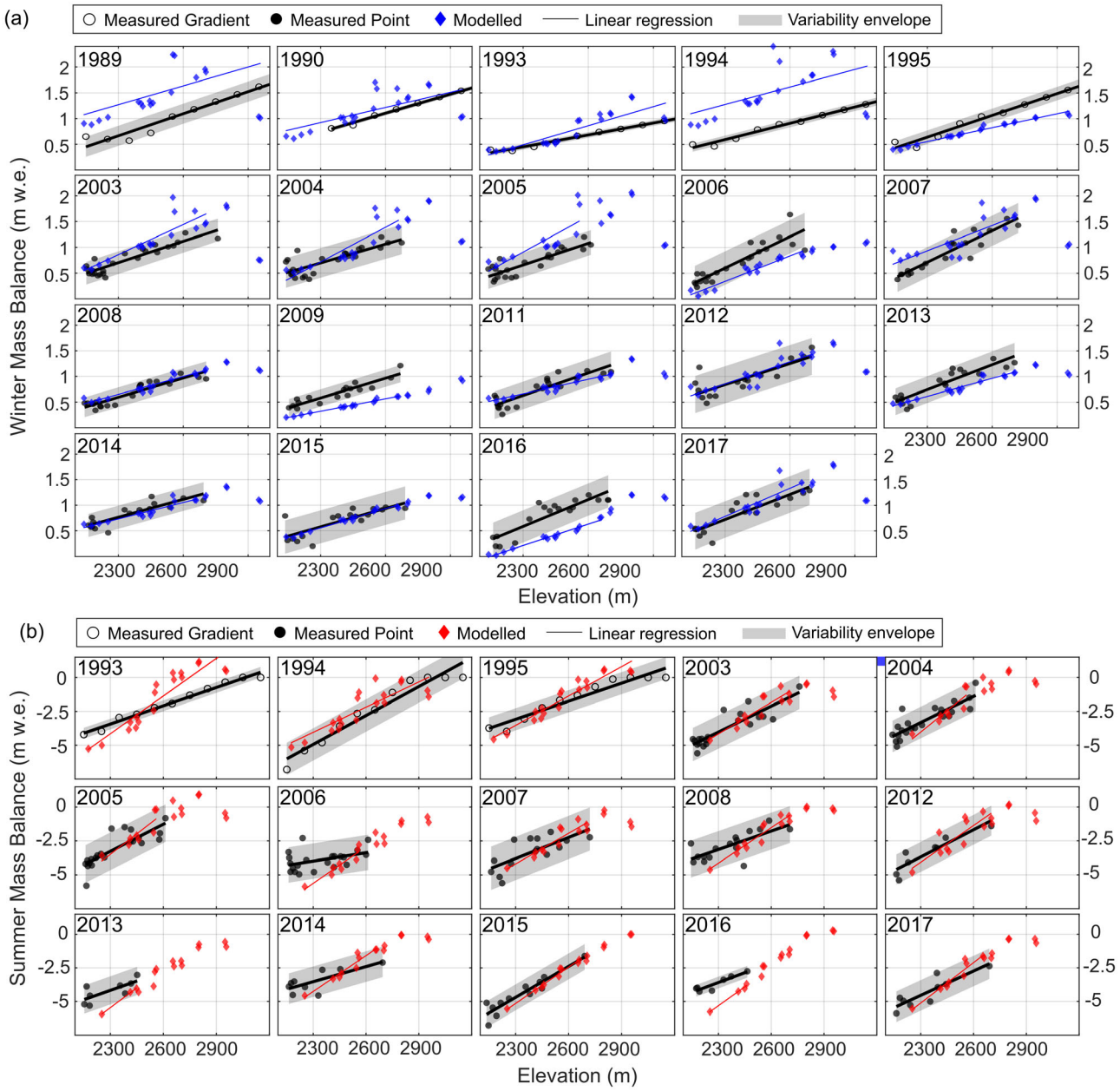

FIGURE 2 Annual measured and modelled point (a) winter and (b) summer mass balance per elevation. The coloured diamonds represent modelled mass balance at individual HRUs, with blue being winter mass balance and red being summer mass balance. The black, filled dots are individual stake measurements, and the empty circles are the measured mass balance gradient.

Where T is the total number of time steps, $x_{sim}(t)$ the simulated streamflow at time t, $x_{obs}(t)$ the observed streamflow at time t, and $\overline{x_{obs}}$ the mean observed discharge. A value of NSE = 1 indicates perfect agreement between simulations and observations whilst NSE = 0 indicates that the model simulations have the same explanatory power as the mean of the observations, and NSE <0 indicates that the model is a worse predictor than the mean of the observations (e.g., Schaefli & Gupta, 2007).

The Kling-Gupta Efficiency (KGE, Gupta et al., 2009) is also used to evaluate model performance:

$$\mathrm{KGE} = 1 - \sqrt{(r-1)^2 + (\alpha-1)^2 + (\beta-1)^2} \tag{3}$$

Where r is the linear correlation between observations and simulations, α is a measure of the flow variability error, and β relates to the bias. KGE can also be written as:

$$\mathrm{KGE} = 1 - \sqrt{(r-1)^2 + \left(\frac{\sigma_{sim}}{\sigma_{obs}} - 1\right)^2 + \left(\frac{\mu_{sim}}{\mu_{obs}} - 1\right)^2} \tag{4}$$

Where σ_{obs} is the standard deviation in observations, σ_{sim} the standard deviation in simulations, μ_{sim} is the simulation mean, and μ_{obs} is the

observation mean. KGE > −0.41 indicates that the simulated variable is performing better than the average of the observations and therefore, the model has predictive power, and a KGE < −0.41 indicates a poor model performance (Knoben et al., 2019). Additionally, the root mean square error (RMSE), the Spearman's rank correlation coefficient (*r*) and the mean bias (MB) are calculated.

2.4 | Assessing trends and variability in hydrometeorological conditions

The presence of significant trends in annual or seasonal air temperature, precipitation and streamflow was assessed using the non-parametric Mann-Kendall significance test at a significance level of alpha = 005. The magnitude of the detected trends was estimated using Sen's slope (Sen, 1968), which calculates the slope using the median of all pairwise slopes in the data set. The seasons for the trend analysis were defined as fall (SON), winter (DJF), spring (MAM) and summer (JJA).

To gain further information on the variability in the streamflow generation processes in the basin, meteorological conditions and melt patterns in years of high streamflow (HF) were compared to those of low streamflow (LF). Years with volumes greater than the mean plus one standard deviation were considered to be high flow (1992, 1994, 2006, 2013, 2015, 2016) and years with volumes less than the mean minus one standard were considered to be low flow (1995, 1996, 1997, 2000, 2003, 2008).

3 | RESULTS

3.1 | Model evaluation

For both the mass balance points available as the mean balance by elevation bands (measured gradient, year 1989–1995 in Figure 2), and for the mass balance points measured at individual stakes (measured point, years 2003–2017 in Figure 2), linear regressions were used to calculate the annual measured mass balance elevation gradient, defined as the rate of change in mass balance with elevation (Figure 2). A variability envelope was calculated as ±2 *SD* around the residuals from the calculated linear regression values (Figure 2a). These variability envelopes were used to assess if the fluctuations from the background elevation gradients were similar between the measured and modelled point mass balance. 77% of the modelled winter mass balances fall within this envelope. In most years, the modelled winter mass balance agrees with the measurements, but for some years, such as 1989, 1994 and 2009, there is minimal overlap between measured and modelled winter mass balance. The calculated and modelled winter mass balance gradients were compared for the 19 available years between 1995 and 2017. The average gradients are similar, with the calculated gradient of 0.14 m.w.e. per 100 m elevation being similar to the modelled gradient of 0.13 m.w.e., with an RMSE of 0.04 m.w.e. per 100 m elevation gain and a correlation coefficient of 0.21. The model has a slight tendency to underestimate the measured gradient with a mean bias of −0.07 m.w.e. The largest difference between modelled and measured winter mass balance occurred at ∼2600 m.a.s.l. and was likely due to the influence of avalanching. Mass balance observations deliberately avoid avalanche-prone areas and so do not reflect this source of variability, even though avalanche deposits have been noted at this elevation in field observations and historical reports (Young, 1977). Therefore, the winter mass balance simulated by CRHM, which account for snow redistribution by gravity, will be more variable than the measured mass balance points at the same elevation. Additionally, evaluation of snow accumulation at the highest elevation HRU is restricted by the lack of measurements above the altitude of 2760 m. Considering that point winter mass balance measurements can vary by up to 0.2 m w.e. over distances of a metre at Peyto Glacier (Demuth & Keller, 2006; Young, 1977), the modelled winter balance is considered to have been simulated in a satisfactory manner.

For summer mass balance, 92% of the modelled values for the 2007–2013 period, or 97 of the 108 values, fit within the variability envelope of the measured stake balances (Figure 2b). Despite most of the modelled values fitting within the range of measured values, the mass balance gradient for summer mass balance was consistently larger than the measured one, with a mean modelled gradient of 0.88 m.w.e. per 100 m elevation gain being larger than the mean modelled rate of 0.54 m.w.e., with an RMSE of 0.39 m.w.e., mean bias of 0.63 m.w.e. and a correlation coefficient of −0.04. The gradient standard deviation is larger for the measurements (0.58 m.w.e.) than for the modelled values (0.38 m.w.e.).

A comparison of modelled snow depth with snow depth measured at the on-ice AWS for the 2011–2020 winters yielded a NSE ranging between 0.49 and 0.84 and a coefficient of determination (R^2) between 0.62 and 0.98 (Figure 3a). For the nine periods with surface melt measurements from the on-ice AWS, which cover a total of 981 days, the correlation coefficient of observations with modelled ice melt at glacier toe is 0.99, with a mean bias of 0.09 m.w.e., a root mean square error (RMSE) of 0.43 m.w.e. and an NSE of 0.90 (Figure 3b–f). Overall, the set of evaluations of modelled snow accumulation and snow and ice ablation shows that the model can appropriately represent snow and ice dynamics on the glacier.

Modelled streamflow at the basin outlet was compared to the measured streamflow for the 2013–2020 melt seasons (Figure 4). Streamflow measurement was only available during the snow-free season and did not allow a model evaluation for the earliest and latest seasonal low flow or melt events. For the eight melt seasons, the simulations compared to observations with a NSE of 0.69, with annual results ranging from 0.41 to 0.87. RMSE for the entire period was 0.98 $m^3\ s^{-1}$, ranging between 0.66 and 1.2 $m^3\ s^{-1}$ and the mean bias ranged from −0.24 to 0.35. The Kling-Gupta efficiency (KGE, Gupta et al., 2009) ranged between 0.09 to 0.45 for individual years and averaged 0.15 for the entire period. When considering the three components of the KGE, the largest values, indicating stronger performance, are found for the bias (β) and relativity term (α), with lower values corresponding to the correlation term *r*. Considering that high

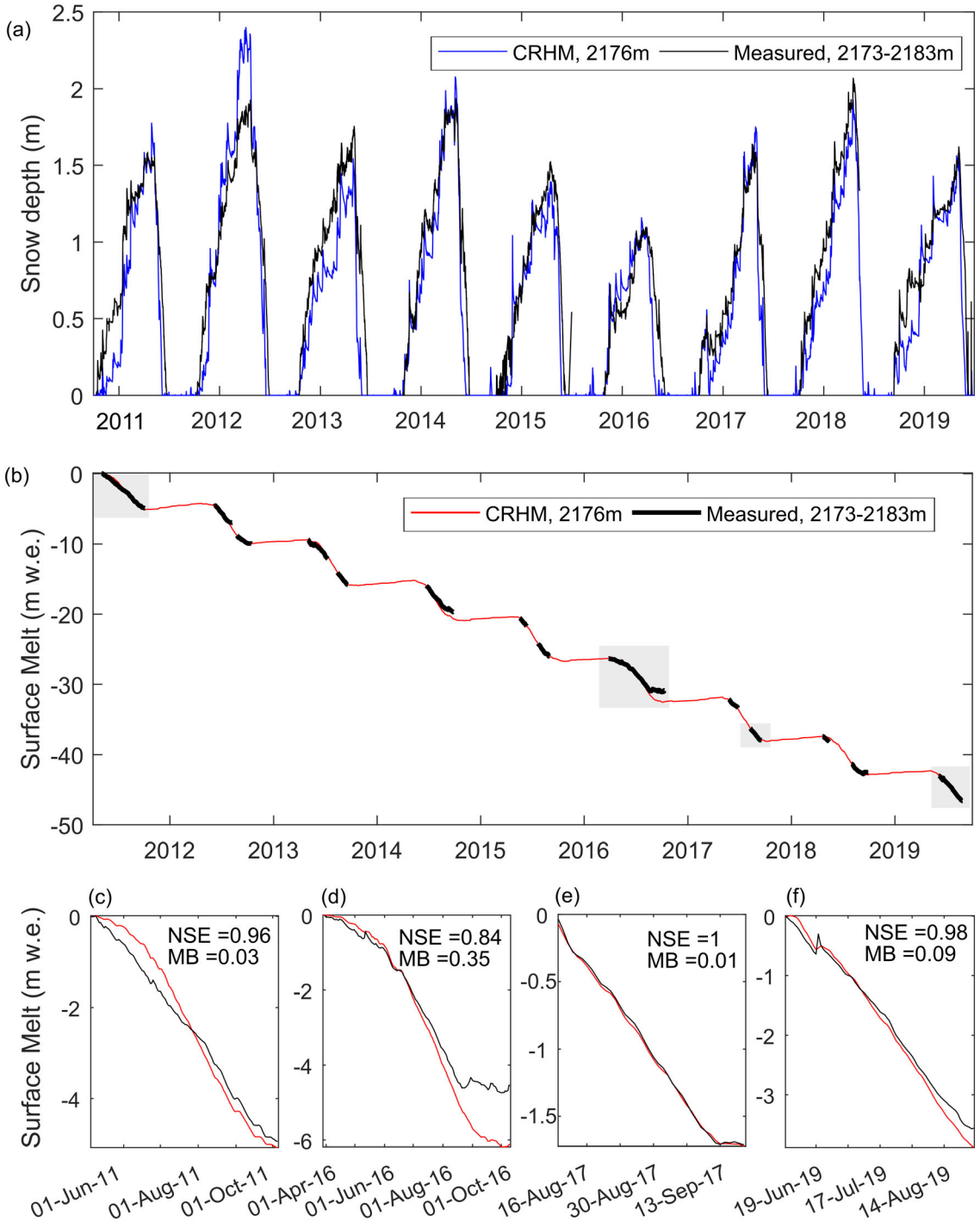

FIGURE 3 Comparison of CRHM model and glacier toe HRU and measurement from the on-ice AWS; (a) snow depth for the 2011–2019 period and (b) cumulative surface melt relative to the start of the observations on 5 May 2011, with the shaded grey areas shown in detail in (c)–(f) with Nash-Sutcliffe efficiency (NSE) and mean bias (MB), also relative to the observation for each period.

NSE values are expected for a basin with a strong seasonal cycle, as demonstrated by Schaefli et al. (2005), and further discussed in Schaefli and Gupta (2007) and Seibert et al. (2018), the NSE performance of the CRHM model was compared with that of a simple benchmark model calculated as the mean observed discharge for each calendar day (DOY average benchmark model, as discussed in Garrick et al., 1978; Schaefli & Gupta, 2007; WMO, 1986). In other words, two NSE values were calculated: a regular NSE with the simulated streamflow, and a benchmark NSE using the DOY average streamflow values. If the benchmark NSE is higher than the regular NSE, then the simulated streamflow shows a lower predictive capacity than the average DOY values. In this case, the DOY average benchmark model performed more poorly than the CRHM model for 7 out of the 8 years available, with its average NSE lower than that of the CRHM model

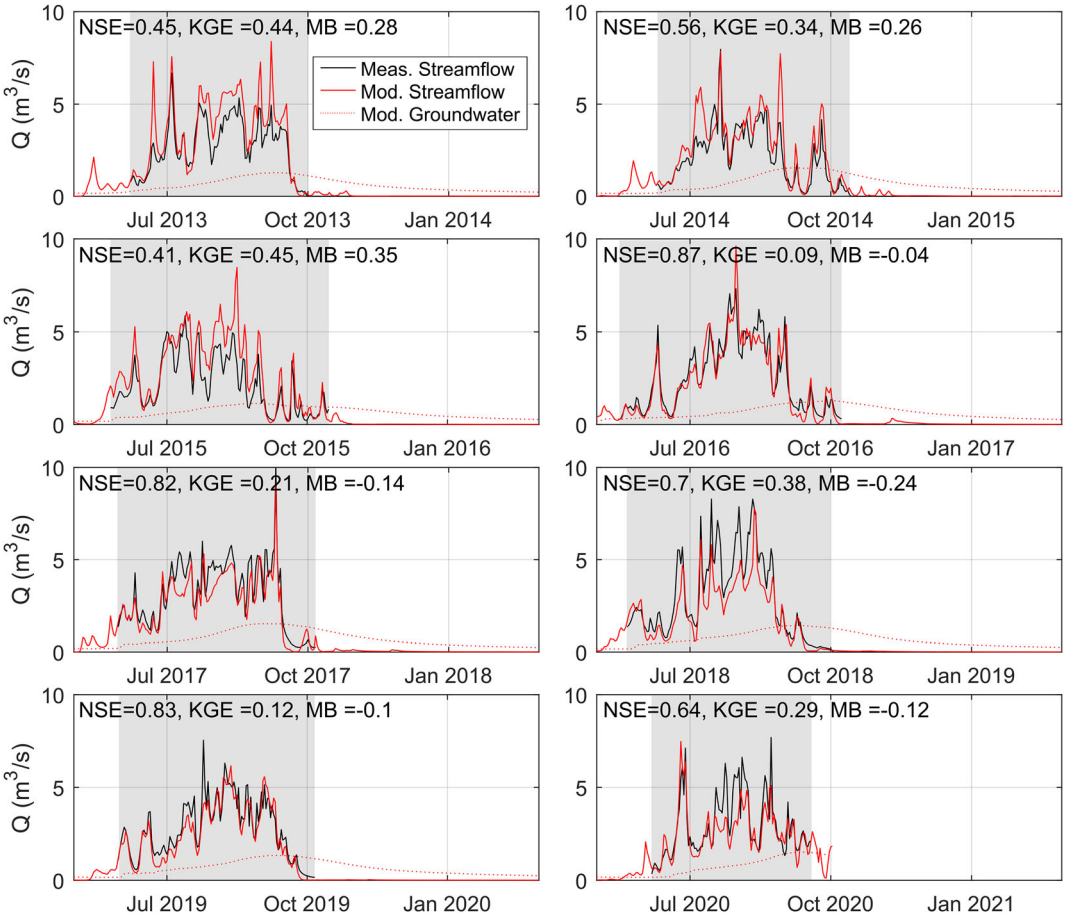

FIGURE 4 Modelled and measured streamflow and simulated groundwater flow for the years 2013–2020. The Nash-Sutcliffe efficiency (NSE), Kling-Gupta efficiency (KGE) and the mean bias (MB) value refer to the agreement between measured and modelled streamflow for the given melt season. The grey overlay indicates the period with streamflow measurements.

by 0.14, providing further evidence that CRHM can capture both the seasonality of the flow regime and the smaller-time scale fluctuations. Modelled groundwater flow is also shown.

3.2 | Basin hydrometeorological variability

3.2.1 | Annual conditions and trends

The basin has a cold climate, with annual mean air temperature staying below 0°C for the whole study period, ranging between −5.0 and −2.3°C (Figure 5a). Only the lowest elevations in the basin, below 2200 m.a.s.l., have an annual mean air temperature above zero, varying from −1.67 to 1.00°C. Summer temperature in the basin can reach up to 23.4°C. The precipitation regime in the basin is dominated by snowfall, which contributes an average of 85% to the total precipitation (Figure 5b). This ratio increases to 89% snowfall in the highest elevation of the basin (above 2700 m.a.s.l.) and decreases to 68% in the lowest elevations (below 2200 m.a.s.l.).

As shown in Figure 5c, annual area-weighted streamflow expressed as water equivalent depth over the PGRB, also known as water yield, varied from 3240 mm yr^{-1}, in 1988, to 1870 mm yr^{-1}, in 1996. On average, snowmelt, both on and off the glacier, contributed the largest volume and fractional contribution, 44%–89%, to annual streamflow. Ice melt from the glacier and ice-cored moraine contributed 10%–45%. Firn melt and rainfall-runoff each contributed 13% or less to annual streamflow, with firn melt ranging from 0%–13% and rainfall-runoff and infiltration contributing 1%–12% of annual streamflow. Rainfall-runoff represents only rainfall on snow-free surfaces (glacier or bare-ground) as rain-on-snow contributes to the snowpack dynamics including refreezing, melting and discharge from the pack depending on the thermodynamic state and porosity of the snowpack. The modelled streamflow components were calculated before the routing routine was applied and therefore, do not reflect streamflow mixing, but runoff sources in the basin. The snow, firn and ice melt originating from the glacier area, grouped as "glacier runoff", provide a disproportionate amount of streamflow, as the glacier covers only 56% of the basin area but the glacier runoff provides on average 71% of annual streamflow. Only two out of the 33 years analysed showed a positive mass balance. For the remaining yearsglacier wastage varied from 6% to 77% of basin yield, with an average of 53%. Glacier wastage was calculated following Comeau et al. (2009) and defined as the

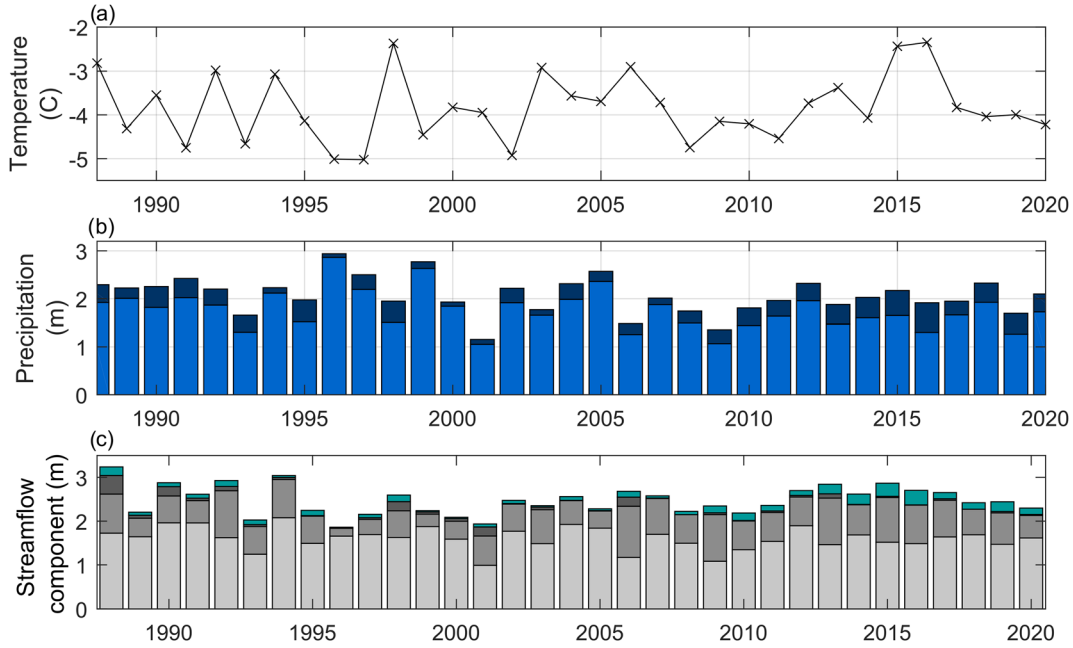

FIGURE 5 Basin area-weighted annual air temperature (a), precipitation (b) and streamflow composition (c), with the total column being annual streamflow in the PGRB for the 1988–2020 period.

volume of ice and firn melt exceeding the annual volume of snow accumulation on the glacier and causing an annual net loss of glacier volume. Basin yield was calculated as the combined streamflow at the basin outlet and groundwater discharge leaving the basin. Surface streamflow at the outlet contributed on average 63% of basin yield, whilst groundwater discharge contributed 37%. The detailed calculate of wastage and shown in Appendix B.

Figure 6 showed significant hydrometeorological trends ($p < 0.05$); at the basin scale, summer temperature increased from 3.50 to 4.55°C over 1988–2020. Over the same time period, winter snowfall decreased by 286 mm, and summer and annual rainfall increased by 179.6 and 152.1 mm respectively. Despite the trends in precipitation phase favouring rainfall, no trends were found in annual air temperature or annual precipitation depth over 1988–2020.

3.2.2 | Seasonal meteorological conditions and streamflow correlation

Further analysis examined the associations between annual streamflow volume and annual and seasonal meteorological variables (temperature, rainfall and snowfall). Annual, spring and summer temperature, summer rainfall and winter snowfall were the only forcing meteorological variables significantly correlated to annual streamflow (Table 2, Figure 7). Winter snowfall was negatively correlated with streamflow, the opposite of what would be expected for a snowmelt-dominated non-glacierized basin. Ice melt, firn melt and rainfall-runoff were the only runoff components significantly correlated to annual streamflow (Table 3, Figure 7). In addition, the timing of the glacier exposure was strongly negatively correlated with streamflow. The timing of ice exposure was quantified as by the day of year (DOY) by which the winter snowpack has fully melted in the mid- and upper glacier area of the basin, with HRU 3 selected as representative. Ice melt and timing of ice exposure were most strongly correlated to the annual streamflow, followed by the rainfall-runoff and firn melt. Even though snowmelt provides the greatest fraction of annual streamflow, no significant correlation was found between snowmelt and streamflow.

In 5 of the 33 years analysed, the snow outside of the glacier area did not completely melt throughout the summer and carried over to the following year. On the glacier, this leftover snow turned to firn, and influenced surface melt in the following summer by having a different albedo and density than either snow or ice. However, the influence of this leftover snow on the following year's streamflow appeared to be minimal in the PGRB as no significant correlation was found between the snow remaining in the basin just before the transition to firn and the following years' streamflow (Table 3).

3.3 | Contrasting high and low streamflow years

High flow years were on average 1.43°C warmer than the years with low flow, with the largest difference in January, March and April (Figure 8a). The HF years received 143 mm more rainfall and 295 mm less snowfall than the LF years, (Figure 8b,c). The differences in precipitation and temperature are reflected in snowpack ablation (Figure 7d). Starting in December, HF and LF snowpack regimes diverge. The HF snowpacks reached a peak SWE of 957 mm in mid-April, whilst the LF snowpacks continued to accumulate until early May when they reached a peak SWE of 1330 mm. Both HF and LF snowpacks follow similar ablation patterns over the melt season and by September 1st, the remaining snowpack starts to transform into

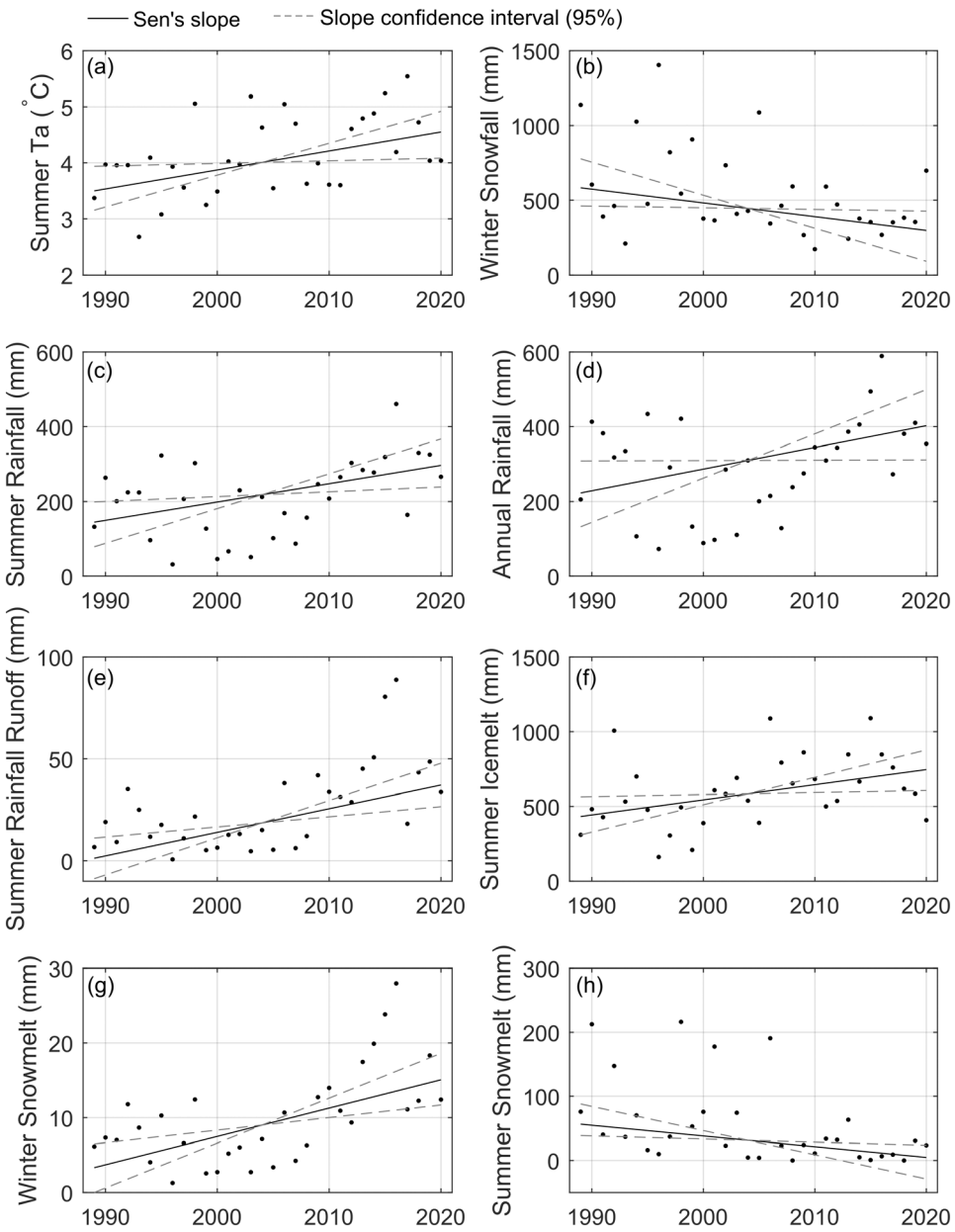

FIGURE 6 Significant trends ($p < 0.05$) for the annual and seasonal basin-averaged hydrometeorological conditions and modelled flow components in the PGRB, calculated for the years 1988–2020. Significant trends were found for summer air temperature, winter snowfall, summer rainfall, annual rainfall, summer rainfall-runoff, summer ice melt, winter snowmelt and summer snowmelt

firn. In LF years, the remaining snowpack was 213 mm SWE at this transition date, whilst in HF years no snow remained. Using the non-parametric Wilcoxon signed rank test (Gibbons & Chakraborti, 2010), the differences in monthly air temperature, snowfall and SWE (but not monthly rainfall) between HF and LF years were significant at the alpha = 0.05 level.

Differences in the sources of streamflow were also analysed between LF and HF years (Figure 9). Annual streamflow volumes were 41% greater in HF years than LF years. Snowmelt provided by far the greatest source of streamflow, but its contribution differed by only 1% between LF and HF years and so did not substantially contribute to interannual variability in streamflow volumes. Differences in snow ablation regime between HF and LF years were apparent; snow ablation started 10 days earlier in HF than in LF years, with rapid melt and depletion of snow occurring 15 days earlier, in mid to late summer. The earlier snow ablation in HF years exposed glacier ice earlier and led to a greater ice exposure by late summer, increasing basin-averaged, late summer ice melt rates from 9 mm d^{-1} in LF to 17 mm d^{-1} in HF years (Figure 9b). As a result, the volume of ice melt was 103% greater in HF than in LF years. Similarly, the firn melt contribution to streamflow was 162% greater in HF compared to LF years, with nearly double the peak melt rate (2.3 compared to 1.4 mm d^{-1}) and an almost one-month earlier start to firn melt. Consistent with greater rainfall, rainfall-runoff was 145% higher in HF years. Even though firn melt and rainfall-runoff were greater in HF years by a larger fraction than other streamflow sources, their enhancement of streamflow was modest as together they contributed less than 10% of streamflow volume. In contrast, ice melt had smaller fractional increases for HF years, but a much stronger impact on differences in streamflow volumes and timing.

LF years were colder, with higher snowfall and lower rainfall. The deeper LF year snowpack combined with a delayed onset to melt due to colder spring temperatures resulted in snowpacks persisting later in

TABLE 2 Spearman rank correlation coefficient (r) and significance (p) for streamflow and meteorological associations.

Variable		Annual streamflow	Fall streamflow	Winter streamflow	Spring streamflow	Summer streamflow
Ta	r	**0.68**	0.21	**0.43**	**0.38**	**0.54**
	α	<0.001	0.265	0.013	0.030	0.001
Rainfall	r	0.33	−0.08	0.09	0.13	**0.38**
	α	0.057	0.677	0.628	0.458	0.03
Snowfall	r	−0.30	−0.21	**−0.36**	0.06	−0.13
	α	0.085	0.235	0.040	0.718	0.450

Note: Significant associations (p < 0.05) are in bold.

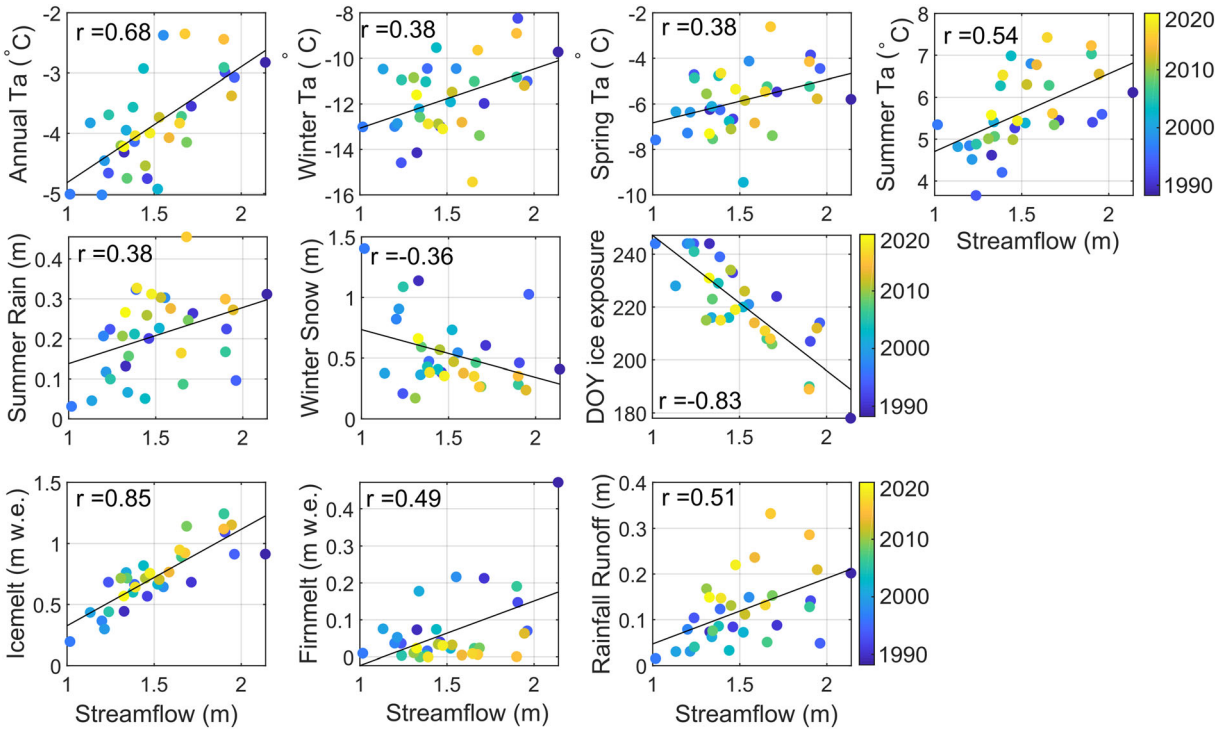

FIGURE 7 Scatterplot for significant associations (shown in bold in Tables 2 and 3) between streamflow and meteorological conditions and streamflow components. The colour of the point refers to the year as shown by the colour bar. The Spearman rank correlation coefficient r is shown in each panel.

the summer in LF than in HF years. This caused less glacier ice to be exposed and ice exposure to occur later in the melt season, such that its melt contributed less to streamflow. Additionally, LF years received lower rainfall. Initial meteorological forcings, differing snow accumulation and depletion patterns, and resulting rates and durations of rainfall-runoff, snowmelt, ice melt and firn melt interacted to cause large streamflow volumetric differences between HF and LF years.

3.4 | Assessing uncertainty of the subsurface storage parameterization

The parameters with the higher uncertainty in the application of the PGRB are the ones associated with non-existent or sparse observations in the basin, preventing the evaluation of these individual processes. This is particularly the case for the surface water-groundwater interactions and the subsurface routing. The surface water-groundwater interactions were parametrized to represent a physical understanding of alpine groundwater systems based on field knowledge from the PGRB and in-depth studies from similar landscapes in the Canadian Rockies, but the lack of direct observations of soil moisture and groundwater storage within PGRB precludes an in-depth evaluation of this model component. Therefore, the uncertainty associated with these parameters was tested. The storage capacity and routing delays of the different land covers, shown in Table 2, were varied and the resulting change in simulated streamflow was assessed in a scenario-based parameter uncertainty assessment (Table 4). Doubling the soil storage decreased streamflow volume by less than 5% and decreasing soil storage by half increased streamflow by 8.8%. However, either doubling or reducing by half the soil storage

volume also influenced the groundwater discharge from the basin, changing both the timing and the total volume of groundwater flow by up to 17% compared to the main simulation. When the soil storage increased whilst the groundwater storage decreased, or the converse, the change in groundwater flow timing and volume was limited to below 4%. However, when the total basin subsurface storage either increased or decreased, groundwater flow changed by up to 30% compared with the baseline simulation. Given the sensitivity of basin groundwater to the subsurface storage parametrization and sparse high elevation groundwater observations, further investigations should assess the transferability of storage parameters for groundwater routing in high alpine basins.

TABLE 3 Spearman rank correlation coefficient (*r*) and significance (*p*) for annual streamflow and annual snowmelt, ice melt, firn melt, rainfall-runoff, peak SWE, the day of year of the glacier ice exposure at elevation 2701 m.a.s.l. (HRU 3) and the end of summer snow in the previous year associations.

	Annual streamflow	
	r	*p*
Snowmelt	−0.03	0.860
Ice melt	**0.85**	**<0.001**
Firn melt	**0.49**	**0.003**
Rainfall runoff	**0.51**	**0.003**
Peak SWE	−0.05	0.779
DOY of ice exposure	**−0.83**	**<0.001**
Previous year unmelted snow	0.05	0.784

Note: Significant associations ($p < 0.05$) are in bold.

4 | DISCUSSION

4.1 | Measurements, process representation and parameter uncertainty

The comprehensive processes in the physically based modelling approach used here were included to reduce model uncertainty; these processes were represented with substantial spatial discretization, and process identification and parametrization were based on extensive fieldwork. In the attempt to comprehensively represent the physical system in the PGRB, it is expected that uncertainty was reduced by selecting appropriate methods and models instead of through more traditional, and sometimes complex, calibration procedures (Clark et al., 2016; Kirchner, 2006). Despite this, model prediction errors can still accrue through inaccuracies in measurements, process representations and parameters (Beven, 2016). The main elements in the modelling procedure relating to these sources of uncertainty are discussed below.

4.1.1 | Limitations of the observational data

A large amount of input data is needed to parametrize and evaluate model simulations but obtaining high-quality observational data from

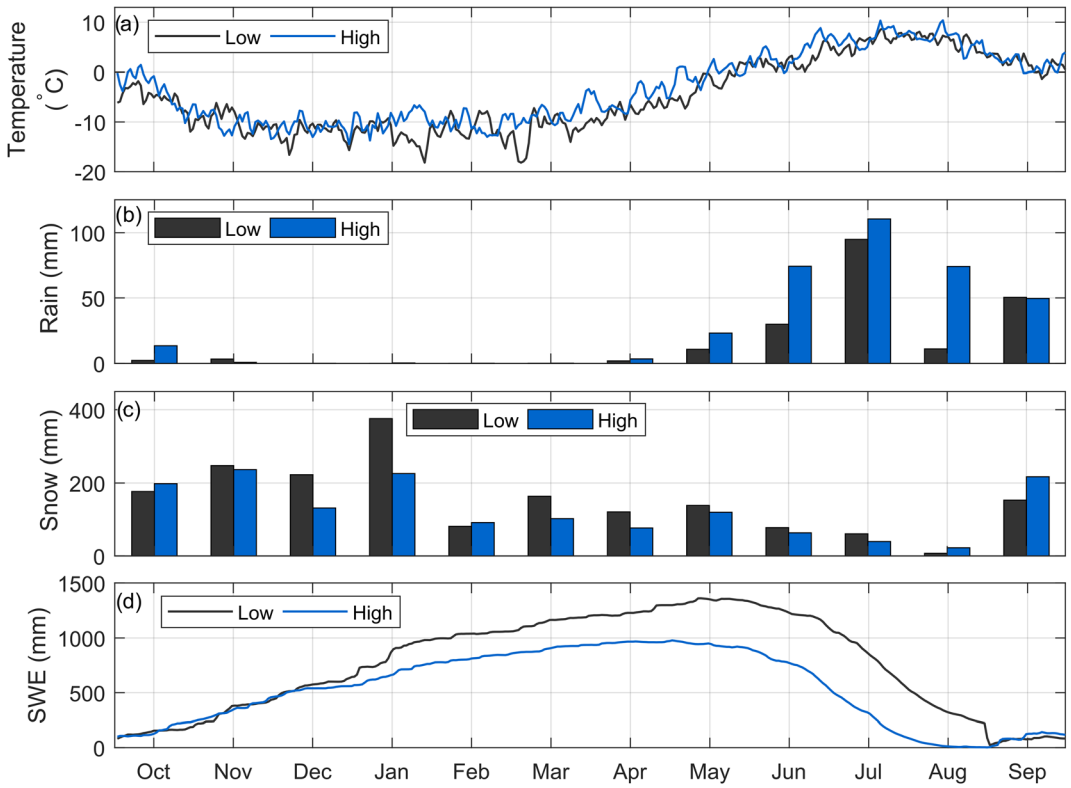

FIGURE 8 Comparison of daily temperature (a), monthly rainfall (b), monthly snowfall (c) and daily snow water equivalent (d) for high streamflow years (light blue) and low streamflow years (dark blue)

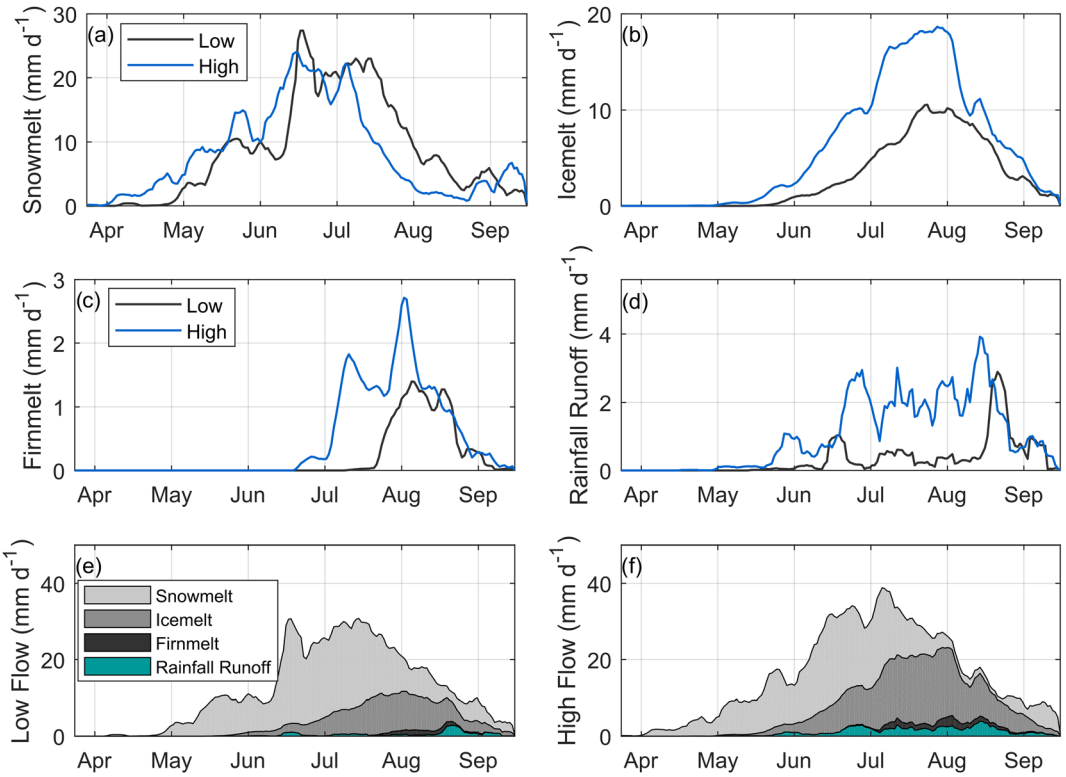

FIGURE 9 Comparison of mean daily basin-averaged streamflow components for high and low streamflow years, with high flow years being the average of 1992, 1994, 2006, 2013, 2015 and 2016 and low streamflow is the average of 1995, 1996, 1997, 2000, 2003, 2008.

TABLE 4 Scenario-based uncertainty assessment for the soil and groundwater storage parameters.

Variable	Soil x2, GW x0.5	Soil x0.5, GW x2	Soil x2, GW x2	Soil x0.5, GW x0.5	Soil x0.5	Soil x2
Streamflow change (%)	−4.5	8.8	−4.5	8.8	8.8	−4.5
Groundwater flow change (%)	−1	3.6	31	−31	−17	−12

remote glacierized mountain basins is an extraordinary challenge. In the PGRB, the long-term meteorological measurements from the network of on-ice stations are invaluable to investigate the temperature patterns across the basin, but the lack of distributed precipitation observations increases uncertainty. Because of this lack of information on the spatial distribution of precipitation, the end-of-winter SWE elevation gradient is used as a proxy for the precipitation elevation gradient. As the SWE elevation gradient considers snow redistribution by wind and gravity, mid-winter melt and sublimation, this approach causes a source of error in the precipitation gradient. Further uncertainty is caused by the use of reanalysis data for precipitation instead of in-situ data. Gridded precipitation datasets are known to be highly uncertain in mountain regions, particularly at high elevations (Henn et al., 2018; Lundquist et al., 2015). Even though the ERA-Interim precipitation was bias-corrected to in-situ observations, ensuring reasonable monthly cumulative volume, the short rainfall events occurring in spring, summer and fall months might have not been adequately captured by the gridded precipitation, resulting in further uncertainty in the model forcing data. Additional measurement of seasonally variable precipitation gradient in the PGRB would be a valuable information to improve model parametrization.

Streamflow information was also limited by the persistence of snowdrifts in the channel, preventing the evaluation of model performance for the early-season and late-season streamflow processes. The uncertainty linked with measuring streamflow in a dynamic, proglacial landscape also increases the uncertainty in developing a robust rating curve, which was mitigated by obtaining several salt-dilution measurements over three melt seasons and a careful assessment of the measurement quality. The simulated glacier winter and summer mass-balances at the higher elevation in the basin are also not well constrained, as there is a lack of measurements at these altitudes due to the difficult access through avalanche and crevassed terrain.

4.1.2 | Limitations in the CRHM process representation and parametrization

The precipitation gradient used is fixed in the model, but there is evidence that mountain precipitation gradients vary seasonally and annually based on the processes controlling the precipitation events (Houze, 2012; Pepin et al., 2022). The lack of temporally variable precipitation gradient could explain the variable performance of the

simulated end-of-winter snow elevation gradient, with some years failing to capture the measured snow accumulation gradient. However, the lack of information on the variability of the precipitation gradient prevented varying this gradient in the modelling framework. The measured mass balance gradient was also more variable than the modelled one, which suggests that elevation has a greater role in controlling melt in the model than is observed. This could be due to deviations from reality in model parameters such as albedo or gradient settings for precipitation and/or temperature and/or other errors.

The meltwater routing through the glacier as applied in this model, a static linear reservoir storage for the snow, firn and ice layer, is a simplification of the complex subglacial and englacial drainage system. Despite its simplicity, the routing approach used here captures the fast drainage of the system at the daily timescale. However, the current configuration of the CRHM glacier melt and routing preclude an analysis of the sub-daily streamflow variation. One option to improve the physical realism of the glacial meltwater routing could be to include a transient storage parametrization based on SWE or time of year to reflect the developing englacial and subglacial drainage system of the glacier, as in Stahl et al. (2008). A combination of dye and hydrochemistry tracing experiments could provide insights in the flow path of meltwater through the glacier system (Fyffe, Brock, Kirkbride, Black, et al., 2019; Fyffe, Brock, Kirkbride, Mair, et al., 2019; Nienow et al., 1998).

Another model improvement that would improve the glacier module process representation would be to implement ice-flow dynamics in the simulations. In this case, the glacier area was constrained by satellite imagery, and the predominantly negative mass balance even at the higher elevation in the basin avoided the infinite accumulation of snow in the accumulation area, a problem that can occur when ice-flow dynamics is not implemented. Further work should be conducted to implement and test an ice flow routine.

The lack of soil moisture and groundwater observations in the basin limit the evaluation of surface water-groundwater interaction and prevents a thorough assessment of the possibility of a "leaky catchment" (Fan, 2019). Groundwater contributions and surface water-groundwater interactions could contribute to the bias in simulated streamflow volumes. The fate of groundwater in alpine basins in the Canadian Rockies has been suggested to be mostly limited to local, shallow aquifers in coarse deposits connecting first- and second-order streams (Hayashi, 2020), but some studies have suggested that glacier basin groundwater recharges regional and mountain block aquifers (Campbell & Ryan, 2021; Castellazzi et al., 2019). Considering both possibilities, the water entering the groundwater system in the PGRB simulations could contribute to unmeasured streamflow just downstream of the basin outlet and contribute to the Peyto Lake water budget or form regional flow networks resurfacing further downstream.

4.2 | PGRB trends and compensatory behaviour

The absence of temporal trends in annual air temperature and precipitation in this study contrast with most findings in the Canadian Rockies (Harder et al., 2015). DeBeer et al. (2016) found a 2°C increase in air temperature and a 14% precipitation increase in this region for the period 1950–2015. Pradhananga and Pomeroy (2022a) contrasted the hydrology of the PGRB between the 1960s and the 2010s and found an increase of 260 mm (16%) in streamflow with a 226 mm (16%) decrease in precipitation. The difference in trends is most likely due to the different periods analysed and the methodologies used. However, for 35 basins in the Columbia River headwaters, located southwest of the PGRB in the adjacent Selkirk and Monashee mountains, Moore et al. (2020) did not find significant trends at $p < 0.05$ in August air temperature for the 1977–2017 period, but found a significant decreasing trend at $p < 0.05$ in August precipitation, which is similar to the trends found for summer rainfall and summer temperature in this study. For streamflow components, significant increasing trends were found for summer rainfall-runoff, summer ice melt, and winter snowmelt, and a decreasing trend was found for summer snowmelt, but no trends were found for seasonal or annual streamflow. This is consistent with Naz et al. (2014), who did not find significant trends in streamflow for the years 1981–2007 for the upper Bow River at Lake Louise, a 422 km^2 basin adjacent to the PGRB. These results contrast with findings by Moore et al. (2020) and Stahl and Moore (2006), who found decreasing trends in August streamflow for glacierized basins in mountain ranges west of the Continental Divide. The difference in these trends might be linked to the different snow accumulation and weather patterns occurring on either side of the Continental Divide; conditions are typically colder and drier on the eastern slopes, but also to the difference in time period analysed (only August versus summer period).

Even if some trends were observed in the summer air temperature, winter snowfall, summer rainfall, and in certain streamflow components in the PGRB, no trend was noticeable in the net annual streamflow volumes. This suggests that, for the period studied, there might be compensating effects amongst the hydrological processes and such that the net flow components generating basin streamflow have been relatively insensitive to environmental change. Harder et al. (2015) found evidence for such cold regions compensatory behaviour in the unglacierized Marmot Creek Research Basin in the Canadian Rockies which dampened its streamflow response to changing climate and land cover. Natural climate variability might also have concealed the streamflow trend, as discussed by Fatichi et al. (2014), who found that natural climate variability obscured climate-driven changes in streamflow by up ±20% in the Alps.

4.3 | Linking PGRB flow variability with hydrological processes

Within the PGRB, the lack of correlation between snowmelt and streamflow, combined with the highly significant correlation of streamflow to summer meteorology, suggests that summer hydrometeorological and glaciological conditions play an important role in governing the inter-annual variability of streamflow. This is consistent with results from Europe by Farinotti et al. (2012) who analysed nine alpine glacierized basins in the Alps and found that annual streamflow

and precipitation were not significantly correlated for basins with glacierized areas over 40%, but that summer air temperature and annual streamflow were well correlated for basins with a glacierized area above 35%. In the highly glacierized Nordic Creek basin, located 85 km west of the PGRB in the Selkirk Mountains of British Columbia, glacier wastage contributions to streamflow were also found to be highly variable year-to-year (Moore et al., 2020).

The influence of winter conditions on streamflow variability was also noticeable through the significant negative correlation of streamflow with winter snowfall and timing of ice exposure rather than snowmelt or peak snow water equivalent. It should be noted that not all snowfall will form snowmelt in high snowfall years and so snowfall is more variable than snowmelt. The negative correlation between winter snowfall and streamflow volume is due to the control that snowfall exerts on the timing of summer ice exposure, as confirmed by the strong negative correlation between timing of ice exposure and streamflow. In low snowfall years, glacier ice is exposed earlier, and due to its lower albedo, the surface melt is enhanced, leading to higher annual streamflow. This correlation is possible when the additional melt from exposed glacier ice in low snowfall years exceeds the reduction in snowmelt from the glacier and non-glacier fractions of the basin.

The variability between low flow years and high flow years was a combination of hydrological processes. In addition to LF years receiving lower rainfall, initial meteorological forcings, differing snow accumulation and depletion patterns, and resulting rates and durations of rainfall-runoff, snowmelt, ice melt and firn melt interacted to cause large streamflow volumetric differences between HF and LF years. This result is consistent with the findings of Pradhananga and Pomeroy (2022a; 2022b) who found that with warming conditions from the 1960s to current times, glacierized basin streamflow in the Canadian Rockies was increasing despite declining precipitation and snowmelt, the difference being sustained by greater ice melt.

4.4 | Comparing flow composition

The flow composition fractions calculated in this study, with snowmelt contributing 44%–89% to annual streamflow, ice melt contributing 10%–45% and firn melt and rainfall-runoff contributing to 13% or less, are consistent with other studies, even though a comparison of streamflow composition between studies is complicated by the range of methods that can be used to define the streamflow components (Frenierre & Mark, 2013), by the varying definitions of "glacier runoff" (Radic & Hock, 2014), and the varying temporal and spatial scale investigated. A previous study by Comeau et al. (2009), conducted on macro-scale basins located in the Canadian Rockies, showed that July–September glacier runoff (snow and ice melt from the glacier area) contributed 73%–83% of the streamflow in basins with more than 10% glacier cover. For the Peyto Creek basin, corresponding to a slightly larger basin than the one investigated in this study, they additionally found that for the 1973–1977 period, glacier wastage flux (or the net glacier water storage lost from negative mass balance) contributed between 48% and 74% of the July–September streamflow, but did not provide annual values due to the lack of streamflow measurements in other months. For the highly glacierized Nordic Creek basin (58% glacier-cover in 2013), Moore et al. (2020), found that the wastage flux contributed from 9%–19% of annual water yield, much lower values than calculated in this study. Further comparison can be made with modelling studies of alpine glacierized basin in other mountain ranges, but caution is needed in interpreting these for comparison due to the difference in climate and modelling methodology. In the Alps, Verbunt et al. (2003) found that in a 47% glacierized basin, the glacier runoff (snow, and ice melt, but not rainfall on the glacier) contributed 62% of total streamflow, with 20% originating from ice melt, 10% from firn melt and 32% from on-glacier snowmelt, but did not indicate the proportion of off-glacier snowmelt contribution to streamflow and therefore underestimated the contribution of snowmelt at the basin scale. The same study also found that for a basin with 69% glacier cover, the glacier runoff contributed 85% of basin streamflow. Gao et al. (2012) found that, in a 44% glacierized basin in Central Asia, 60% of the basin streamflow originated from the glacierized area, which includes firn, snow and ice melt and liquid routed on the glacier surface. These proportions of on-glacier runoff contribution to streamflow are comparable to the results from the PGRB, where 71% of annual runoff originates from the glacier area (including firn melt, snowmelt, ice melt and rainfall on the glacier), which covers 56% of the basin. In the Andes, Burger et al. (2019) found that in a basin with 16% glacier cover, snowmelt on and off the glacier contributed 66%–93% of basin streamflow, ice melt formed 3.5%–32%, and rainfall-runoff did not exceed 6%. Therefore, the numbers presented here are within the ranges of values obtained in highly glacierized alpine basins, but the different approaches to computing flow compositions and glacier runoff contribution to streamflow preclude deeper comparisons between different studies. To facilitate future comparison between hydrological studies in mountain basins, the glacio-hydrological community should define common and clear metrics to compare runoff components, including both on and off-glacier runoff components and glacier wastage contributions to streamflow.

5 | CONCLUSIONS

Streamflow generation in a glacierized mountain catchment such as the PGRB is caused by a complex interplay of hydrological processes. This study aimed to investigate the key sources of inter-annual streamflow variability in a highly glacierized basin. To do so, a process-oriented, physically based glacier hydrological model was created in the Cold Regions Hydrological Modelling Platform to represent the full range of processes generating streamflow in a small glacierized Canadian Rockies headwater basin for the period 1990–2020. By using parameters derived from fieldwork, literature values or physical principles, the model was able to capture the basin's snow accumulation, ice and snow melt patterns, and streamflow well. These modelling results emphasize the importance of long-term in-situ

observations of meteorological variables in remote, high altitude glacierized basin to guide and evaluate model application.

Even though trends were obtained in selected meteorological forcings in the PGRB (summer air temperature, summer and annual rainfall and winter snowfall), these trends did not translate into trends in streamflow or runoff components. The predominance of interannual variability in the glacierized basin streamflow was due to hydrometeorological factors that affected ice melt with much smaller impacts from firn melt and rainfall-runoff. Annual streamflow was significantly correlated with annual air temperature, as well as summer rainfall and winter snowfall. The negative correlation with winter snowfall and with timing of ice exposure, concomitant with the lack of association between snowmelt and streamflow indicates that winter conditions play a role in streamflow variability by regulating subsequent summer ice exposure and albedo in the PGRB. Lower snowfall reduces summer albedo on the glacier. Snowmelt, whilst generating a larger fraction of streamflow, was a small source of interannual streamflow variability because high snowfall years were also low ice melt years due to the impact of deep snowpack in covering and protecting glacier ice from melting until late in the summer.

A comparison of high and low streamflow years showed that streamflow in high flow years was 41% greater than in low flow years. High flow years were warmer (+1.43°C), rainier (+145 mm) and less snowy (−295 mm w.e.) than low flow years. These differences in temperature and precipitation caused earlier snowmelt (−10 days), enhanced ice melt (+103%) and firn melt (+162%), and greater rainfall-runoff (+146%). As low snowfall years were warmer and rainier years than high snowfall years, rainfall and firn melt runoff sources also increased with ice melt in these years. High snowfall did not necessarily translate into high snowmelt, as in high snowfall years not all the snow melted. These compensatory feedbacks between snow and glacier runoff processes affected both interannual variability and long-term trends.

This assessment of trends in the PGRB combined with an analysis of the correlation between meteorological conditions and streamflow and a diagnosis of the hydrometeorological conditions resulting in high and low flow years revealed the key drivers of streamflow variability in the PGRB but also highlighted the complexities of streamflow generation in mountain catchments.

Considering that meteorological extremes are expected to increase in the future, and that glacier retreat enhances flow variability by changing the streamflow regime from ice-dominated to snowmelt and rainfall-runoff dominated, the streamflow in headwater glacierized basins is expected to continue to change in the upcoming decades. Increasingly warm conditions may cause an increase in the frequency of high flow conditions whilst glacier coverage still remains, much as was noted in the shift from the 1960s to recent years by Pradhananga and Pomeroy (2022a). These future changes will be superimposed on the current inter-annual variability that currently dominates the streamflow response in the PGRB. To understand and robustly predict the changing water supply from in glacierized mountain basins, it is crucial to consider the complex interplay of streamflow generation processes.

ACKNOWLEDGEMENTS

The authors wish to thank the Natural Sciences Engineering and Research Council of Canada Discovery Grants and Vanier and Michael Smith Scholarships, the Canada Foundation for Innovation, Canada Research Chairs programme and the Canada First Research Excellence Fund's Global Water Futures programme for support. Peyto Glacier Research Basin has been maintained by many people over the years including most recently, Mike Demuth and Mark Ednie of Natural Resources Canada, and May Guan, Angus Duncan, Eric Courtin and Greg Galloway of the Centre for Hydrology, University of Saskatchewan. We thank Dan Moore and an additional reviewer for their helpful and thorough comments on the manuscript.

DATA AVAILABILITY STATEMENT

The CRHM modelling files (observation and project files), as well as the scripts used to analyze and plot the CRHM model outputs, can be found at: https://github.com/caubrywake/PeytoCRHM_1990_2020.

ORCID

Caroline Aubry-Wake https://orcid.org/0000-0002-9452-8580
John W. Pomeroy https://orcid.org/0000-0002-4782-7457

REFERENCES

Aubry-Wake, C., Lamontagne-Hallé, P., Baraër, M., McKenzie, J. M., & Pomeroy, J. W. (2022). Using ground-based thermal imagery to estimate debris thickness over glacial ice: Fieldwork considerations to improve the effectiveness. *Journal of Glaciology*, 1–17. DOIi:10.1017/jog.2022.67

Ayers, H. D. (1959). Influence of soil profile and vegetation characteristic on net rainfall supply to runoff. In *Spillway design floods: Proceeding of hydrology symposium No. 1*. National Research Council of Canada. 198–205.

Beniston, M. (2003). Climatic change in mountain regions: A review of possible impacts. In *Climatic change* (pp. 5–31). Kluwer Academic Publishers. https://doi.org/10.1023/A:1024458411589

Benn, D. I., & Evans, D. J. A. (2010). *Glaciers and glaciation* (2nd ed.). Routledge.

Bernhardt, M., & Schulz, K. (2010). SnowSlide: A simple routine for calculating gravitational snow transport. *Geophysical Research Letters*, *37*(11), 1–6. https://doi.org/10.1029/2010GL043086

Bernhardt, M., Schulz, K., Liston, G. E., & Zängl, G. (2012). The influence of lateral snow redistribution processes on snow melt and sublimation in alpine regions. *Journal of Hydrology*, *424–425*, 196–206. https://doi.org/10.1016/j.jhydrol.2012.01.001

Beven, K. (2006). A manifesto for the equifinality thesis. *Journal of Hydrology*, *320*(1–2), 18–36. https://doi.org/10.1016/j.jhydrol.2005.07.007

Beven, K. (2016). Facets of uncertainty: E pistemic uncertainty, non-stationarity, likelihood, hypothesis testing, and communication. *Hydrological Sciences Journal*, *61*(9), 1652–1665. https://doi.org/10.1080/02626667.2015.1031761

Burger, F., Ayala, A., Farias, D., Shaw, T. E., MacDonell, S., Brock, B., McPhee, J., & Pellicciotti, F. (2019). Interannual variability in glacier contribution to runoff from a high-elevation Andean catchment: Understanding the role of debris cover in glacier hydrology. *Hydrological Processes*, *33*(2), 214–229. https://doi.org/10.1002/HYP.13354

Campbell, É. M. S., & Ryan, M. C. (2021). Nested recharge systems in mountain block hydrology: High-elevation snowpack generates low-elevation overwinter baseflow in a Rocky Mountain river. *Water*, *13*(16), 2249. https://doi.org/10.3390/W13162249

Carenzo, M., Pellicciotti, F., Mabillard, J., Reid, T., & Brock, B. W. (2016). An enhanced temperature index model for debris-covered glaciers accounting for thickness effect. *Advances in Water Resources*, *94*, 457–469. https://doi.org/10.1016/j.advwatres.2016.05.001

Castellazzi, P., Burgess, D., Rivera, A., Huang, J., Longuevergne, L., & Demuth, M. N. (2019). Glacial melt and potential impacts on water resources in the Canadian Rocky Mountains. *Water Resources Research*, *55*(12), 10191–10217. https://doi.org/10.1029/2018WR024295

Chen, J., & Ohmura, A. (1990). *Estimation of Alpine glacier water resources and their change since the 1870s* (Vol. 193, pp. 127–135). IAHS Publications.

Chernos, M., MacDonald, R. J., Nemeth, M. W., & Craig, J. R. (2020). Current and future projections of glacier contribution to streamflow in the upper Athabasca River Basin. *Canadian Water Resources Journal / Revue Canadienne Des Ressources Hydriques*, *45*(4), 324–344. https://doi.org/10.1080/07011784.2020.1815587

Clark, C. O. (1945). Storage and the unit hydrograph. *Proceedings of the American Society of Civil Engineers*, *69*, 1419–1447.

Clarke, G. K. C., Jarosch, A. H., Anslow, F. S., Radić, V., & Menounos, B. (2015). Projected deglaciation of western Canada in the twenty-first century. *Nature Geoscience*, *8*(5), 372–377. https://doi.org/10.1038/ngeo2407

Clark, M. P., Wilby, R. L., Gutmann, E. D., Vano, J. A., Gangopadhyay, S., Wood, A. W., Fowler, H. J., Prudhomme, C., Arnold, J. R., & Brekke, L. D. (2016). Characterizing uncertainty of the hydrologic impacts of climate change. *Current Climate Change Reports*, *2*(2), 55–64. https://doi.org/10.1007/S40641-016-0034-X/FIGURES/1

Clow, D. W., Schrott, L., Webb, R., Campbell, D. H., Torizzo, A., & Dornblaser, M. (2003). Ground water occurrence and contributions to streamflow in an slpine catchment, Colorado Front Range. *Groundwater*, *41*(7), 937–950. https://doi.org/10.1111/j.1745-6584.2003.tb02436.x

Comeau, L., Al, P. A., & Demuth, M. N. (2009). Glacier contribution to the North and South Saskatchewan Rivers. *Hydrological Processes*, *23*(18), 2640–2653. https://doi.org/10.1002/hyp

DeBeer, C. M., & Pomeroy, J. W. (2009). Modelling snow melt and snowcover depletion in a small alpine cirque, Canadian Rocky Mountains. *Hydrological Processes*, *23*(18), 2584–2599. https://doi.org/10.1002/hyp.7346

DeBeer, C. M., Wheater, H. S., Carey, S. K., & Chun, K. P. (2016). Recent climatic, cryospheric, and hydrological changes over the interior of western Canada: A review and synthesis. *Hydrology and Earth System Sciences*, *20*(4), 1573–1598. https://doi.org/10.5194/hess-20-1573-2016

Dee, D. P., Uppala, S. M., Simmons, A. J., Berrisford, P., Poli, P., Kobayashi, S., Andrae, U., Balmaseda, M. A., Balsamo, G., Bauer, P., Bechtold, P., Beljaars, A. C. M., van de Berg, L., Bidlot, J., Bormann, N., Delsol, C., Dragani, R., Fuentes, M., Geer, A. J., … Vitart, F. (2011). The ERA-Interim reanalysis: Configuration and performance of the data assimilation system. *Quarterly Journal of the Royal Meteorological Society*, *137*(656), 553–597. https://doi.org/10.1002/qj.828

Demuth, M. N., & Keller, R. (2006). An assessment of the mass balance of Peyto glacier (1966-1995) and its relation to recent and past-century climatic variability. In M. N. Demuth, D. S. Munro, & G. J. Young (Eds.), *Peyto glacier: One century of science. National Hydrology Research Institute Science Report 8* (pp. 83–132). National Hydrology Research Institute Science report 8.

Demuth, M. N., Munro, D. S., & Young, G. J. (2006). *Peyto glacier: One century of science*. National Hydrology Research Institute.

Duethmann, D., Bloschl, G., & Parajka, J. (2020). Why does a conceptual hydrological model fail to correctly predict discharge changes in response to climate change? *Hydrology and Earth System Sciences*, *24*(7), 3493–3511. https://doi.org/10.5194/HESS-24-3493-2020

Dyurgerov, M. B. (2002). *Glacier mass balance and regime: Data of measurement and analysis* (Vol. 55, pp. 1–268). Institute of Arctic and Alpine Research. Occasional Paper 55, University of Colorado.

Essery, R., & Etchevers, P. (2004). Parameter sensitivity in simulations of snowmelt. *Journal of Geophysical Research*, *109*(D20111), 1–15. https://doi.org/10.1029/2004JD005036

Fan, Y. (2019). Are catchments leaky? *WIREs Water*, *6*(6), 1–25. https://doi.org/10.1002/wat2.1386

Fang, X., Pomeroy, J. W., Ellis, C. R., MacDonald, M. K., DeBeer, C. M., & Brown, T. (2013). Multi-variable evaluation of hydrological model predictions for a headwater basin in the Canadian Rocky Mountains. *Hydrology and Earth System Sciences*, *17*(4), 1635–1659. https://doi.org/10.5194/hess-17-1635-2013

Farinotti, D., Usselmann, S., Huss, M., Bauder, A., & Funk, M. (2012). Runoff evolution in the Swiss Alps: Projections for selected high-alpine catchments based on ENSEMBLES scenarios. *Hydrological Processes*, *26*(13), 1909–1924. https://doi.org/10.1002/hyp.8276

Fatichi, S., Rimkus, S., Burlando, P., & Bordoy, R. (2014). Does internal climate variability overwhelm climate change signals in streamflow? The upper Po and Rhone basin case studies. *Science of The Total Environment*, *493*, 1171–1182. https://doi.org/10.1016/j.scitotenv.2013.12.014

Finger, D., Pellicciotti, F., Konz, M., Rimkus, S., & Burlando, P. (2011). The value of glacier mass balance, satellite snow cover images, and hourly discharge for improving the performance of a physically based distributed hydrological model. *Water Resources Research*, *47*(7). https://doi.org/10.1029/2010wr009824

Fountain, A. G., & Tangborn, W. V. (1985). The Effect of glaciers on streamflow variations. *Water Resources Research*, *21*(4), 579–586. https://doi.org/10.1029/WR021i004p00579

Frans, C., Istanbulluoglu, E., Lettenmaier, D. P., Fountain, A. G., & Riedel, J. (2018). Glacier recession and the response of summer streamflow in the Pacific Northwest United States, 1960–2099. *Water Resources Research*, *54*(9), 6202–6225. https://doi.org/10.1029/2017WR021764

Frenierre, J. L., & Mark, B. G. (2013). A review of methods for estimating the contribution of glacial meltwater to total watershed discharge. *Progress in Physical Geography*, *38*(2), 173–200. https://doi.org/10.1177/0309133313516161

Freudiger, D., Kohn, I., Seibert, J., Stahl, K., & Weiler, M. (2017). Snow redistribution for the hydrological modeling of alpine catchments. *Wiley Interdisciplinary Reviews: Water*, *4*(5), e1232. https://doi.org/10.1002/wat2.1232

Fyffe, C. L., Brock, B. W., Kirkbride, M. P., Black, A. R., Smiraglia, C., & Diolaiuti, G. (2019). The impact of supraglacial debris on proglacial runoff and water chemistry. *Journal of Hydrology*, *576*, 41–57. https://doi.org/10.1016/J.JHYDROL.2019.06.023

Fyffe, C. L., Brock, B. W., Kirkbride, M. P., Mair, D. W. F., Arnold, N., Smiraglia, C., Diolaiuti, G., & Diotri, F. (2019). Do debris-covered glaciers demonstrate distinctive hydrological behaviour compared to clean glaciers? *Journal of Hydrology*, *570*, 584–597. https://doi.org/10.1016/j.jhydrol.2018.12.069

Gao, H., He, X., Ye, B., & Pu, J. (2012). Modeling the runoff and glacier mass balance in a small watershed on the Central Tibetan Plateau, China, from 1955 to 2008. *Hydrological Processes*, *26*(11), 1593–1603. https://doi.org/10.1002/hyp.8256

Garnier, B., & Ohmura, A. (1970). The evaluation of surface variations in solar radiation income. *Solar Energy*, *13*, 21–34. https://doi.org/10.1016/0038-092X(70)90004-6

Garrick, M., Cunnane, C., & Nash, J. E. (1978). A criterion of efficiency for rainfall-runoff models. *Journal of Hydrology*, *36*, 375–381. https://doi.org/10.1016/0022-1694(78)90155-5

Gibbons, J. D., & Chakraborti, S. (2010). *Nonparametric statistical inference*. Chapman and Hall/CRC. https://doi.org/10.5005/jp/books/10313_14

Gray, D. M., Toth, B., Zhao, L., Pomeroy, J. W., & Granger, R. J. (2001). Estimating areal snowmelt infiltration into frozen soils. *Hydrological Processes*, *15*(16), 3095–3111. https://doi.org/10.1002/hyp.320

Grisogono, B., & Oerlemans, J. (2001). A theory for the estimation of surface fluxes in simple katabatic flows. *Quarterly Journal of the Royal Meteorological Society*, *127*(578), 2725–2739. https://doi.org/10.1002/qj.49712757811

Gruber, S., & Haeberli, W. (2009). Mountain permafrost. In *Permafrost soils* (pp. 33–44). Springer Berlin Heidelberg. https://doi.org/10.1007/978-3-540-69371-0_3

Gupta, H. V., Kling, H., Yilmaz, K. K., & Martinez, G. F. (2009). Decomposition of the mean squared error and NSE performance criteria: Implications for improving hydrological modelling. *Journal of Hydrology*, *377*(1–2), 80–91. https://doi.org/10.1016/j.jhydrol.2009.08.003

Hanzer, F., Helfricht, K., Marke, T., & Strasser, U. (2016). Multilevel spatiotemporal validation of snow/ice mass balance and runoff modeling in glacierized catchments. *The Cryosphere*, *10*(4), 1859–1881. https://doi.org/10.5194/TC-10-1859-2016

Harder, P., & Pomeroy, J. W. (2013). Estimating precipitation phase using a psychrometric energy balance method. *Hydrological Processes*, *27*(May), 1901–1914. https://doi.org/10.1002/hyp.9799

Harder, P., Pomeroy, J. W., & Westbrook, C. J. (2015). Hydrological resilience of a Canadian Rockies headwaters basin subject to changing climate, extreme weather, and forest management. *Hydrological Processes*, *29*(18), 3905–3924. https://doi.org/10.1002/hyp.10596

Hayashi, M. (2020). Alpine hydrogeology: The critical role of groundwater in sourcing the headwaters of the wGorld. *Groundwater*, *58*(4), 498–510. https://doi.org/10.1111/GWAT.12965

Henn, B., Newman, A. J., Livneh, B., Daly, C., & Lundquist, J. D. (2018). An assessment of differences in gridded precipitation datasets in complex terrain. *Journal of Hydrology*, *556*, 1205–1219. https://doi.org/10.1016/J.JHYDROL.2017.03.008

Huss, M., Jouvet, G., Farinotti, D., & Bauder, A. (2010). Future high-mountain hydrology: a new parameterization of glacier retreat. *Hydrology and Earth System Sciences*, *14*(5), 815–829. https://doi.org/10.5194/hess-14-815-2010

Hock, R. (1999). A distributed temperature-index ice- and snowmelt model including potential direct solar radiation. *Journal of Glaciology*, *45*(149), 101–111. https://doi.org/10.1017/S0022143000003087

Hock, R. (2003). Temperature index melt modelling in mountain areas. *Journal of Hydrology*, *282*(1–4), 104–115. https://doi.org/10.1016/s0022-1694(03)00257-9

Hock, R., & Holmgren, B. (2005). A distributed surface energy-balance model for complex topography and its application to Storglaciären, Sweden. *Journal of Glaciology*, *51*(172), 25–36. https://doi.org/10.3189/172756505781829566

Hock, R. (2005). Glacier melt: A review of processes and their modelling. *Progress in Physical Geography*, *29*(3), 362–391. https://doi.org/10.1191/0309133305pp453ra

Hock, R., & Noetzli, C. (1997). Areal melt and discharge modelling of Storglaciären, Sweden. *Annals of Glaciology*, *24*, 211–216. https://doi.org/10.1017/s0260305500012192

Hood, J. L., & Hayashi, M. (2015). Characterization of snowmelt flux and groundwater storage in an alpine headwater basin. *Journal of Hydrology*, *521*, 482–497. https://doi.org/10.1016/j.jhydrol.2014.12.041

Hopkinson, C., Demuth, M. N., & Sitar, M. (2012). *Hydrological implications of periglacial expansion in the Peyto Glacier catchment, Canadian Rockies* (Vol. 352, pp. 341–344). International Association for the Hydrological Sciences/*IUGG Redbook Publication*.

Hopkinson, C., & Young, G. J. (1998). The effect of glacier wastage on the flow of the Bow River at Banff, Alberta, 1951-1993. *Hydrological Processes*, *12*(10–11), 1745–1762. https://doi.org/10.1002/(SICI)1099-1085(199808/09)12:10/11<1745::AID-HYP692>3.0.CO;2-S

Houze, R. A. (2012). Orographic effects on precipitating clouds. *Reviews of Geophysics*, *50*(1), 1001. https://doi.org/10.1029/2011RG000365

Hugonnet, R., McNabb, R., Berthier, E., Menounos, B., Nuth, C., Girod, L., Farinotti, D., Huss, M., Dussaillant, I., Brun, F., & Kääb, A. (2021). Accelerated global glacier mass loss in the early twenty-first century. *Nature*, *592*(7856), 726–731. https://doi.org/10.1038/s41586-021-03436-z

Huss, M., Bookhagen, B., Huggel, C., Jacobsen, D., Bradley, R. S. S., Clague, J. J. J., Vuille, M., Buytaert, W., Cayan, D. R. R., Greenwood, G., Mark, B. G., Milner, A. M., Weingartner, R., & Winder, M. (2017). Toward mountains without permanent snow and ice. *Earth's Future*, *5*(5), 418–435. https://doi.org/10.1002/2016EF000514

Immerzeel, W. W., van Beek, L. P. H., & Bierkens, M. F. P. (2010). Climate change will affect the asian water towers. *Science*, *328*(5984), 1382–1385. https://doi.org/10.1126/science.1183188

Jansson, P., Hock, R., & Schneider, T. (2003). The concept of glacier storage: A review. *Journal of Hydrology*, *282*(1–4), 116–129. https://doi.org/10.1016/S0022-1694(03)00258-0

Jost, G., Moore, R. D., Menounos, B., & Wheate, R. (2012). Quantifying the contribution of glacier runoff to streamflow in the upper Columbia River Basin, Canada. *Hydrology and Earth System Sciences*, *16*(3), 849–860. https://doi.org/10.5194/hess-16-849-2012

Kirchner, J. W. (2006). Getting the right answers for the right reasons: Linking measurements, analyses, and models to advance the science of hydrology. *Water Resources Research*, *42*(3), 1–5. https://doi.org/10.1029/2005WR004362

Knoben, W. J. M., Freer, J. E., & Woods, R. A. (2019). Technical note: Inherent benchmark or not? Comparing Nash-Sutcliffe and Kling-Gupta efficiency scores. *Hydrology and Earth System Sciences*, *23*(10), 4323–4331. https://doi.org/10.5194/hess-23-4323-2019

Koboltschnig, G. R., & Schöner, W. (2011). The relevance of glacier melt in the water cycle of the Alps: The example of Austria. *Hydrology and Earth System Sciences*, *15*(6), 2039–2048. https://doi.org/10.5194/hess-15-2039-2011

Krogh, S. A., Pomeroy, J. W., & McPhee, J. (2015). Physically based mountain hydrological modeling using reanalysis aata in Patagonia. *Journal of Hydrometeorology*, *16*(1), 172–193. https://doi.org/10.1175/JHM-D-13-0178.1

Langston, G., Bentley, L. R., Hayashi, M., Mcclymont, A. F., & Pidlisecky, A. (2011). Internal structure and hydrological functions of an alpine proglacial moraine. *Hydrological Processes*, *25*, 2967–2982. https://doi.org/10.1002/hyp.8144

López-Moreno, J.-I., Gascoin, S., Herrero, J., Sproles, E. A., Pons, M., Alonso-González, E., Hanich, L., Boudhar, A., Musselman, K. N., Molotch, N. P., Sickman, J., & Pomeroy, J. (2017). Different sensitivities of snowpacks to warming in Mediterranean climate mountain areas. *Environmental Research Letters*, *12*(7), 74006. https://doi.org/10.1088/1748-9326/aa70cb

López-Moreno, J.-I., Pomeroy, J. W., Alonso-González, E., Morán-Tejeda, E., Revuelto-Benedí, J., & Revuelto, J. (2020). Decoupling of warming mountain snowpacks from hydrological regimes. *Environmental Research Letters*, *15*(11), 114006. https://doi.org/10.1088/1748-9326/abb55f

Lundquist, J. D., Hughes, M., Henn, B., Gutmann, E. D., Livneh, B., Dozier, J., & Neiman, P. (2015). High-elevation precipitation patterns: Using snow measurements to assess daily gridded datasets across the Sierra Nevada, California. *Journal of Hydrometeorology*, *16*(4), 1773–1792. https://doi.org/10.1175/JHM-D-15-0019.1

MacDonald, M. K., Pomeroy, J. W., & Pietroniro, A. (2009). Parameterizing redistribution and sublimation of blowing snow for hydrological models: Tests in a mountainous subarctic catchment. *Hydrological Processes*, *23*(18), 2570–2583. https://doi.org/10.1002/hyp.7356

MacDonald, M. K., Pomeroy, J. W., & Pietroniro, A. (2010). On the importance of sublimation to an alpine snow mass balance in the Canadian Rocky Mountains. *Hydrology and Earth System Sciences*, *14*(7), 1401–1415. https://doi.org/10.5194/hess-14-1401-2010

Marks, D., Domingo, J., Susong, D., Link, T. E., & Garen, D. (1999). A spatially distributed energy balance snowmelt model for application in mountain basins. *Hydrological Processes*, *13*(12–13), 1935–1959. https://doi.org/10.1002/(SICI)1099-1085(199909)13:12/13<1935::AID-HYP868>3.0.CO;2-C

McClung, D. M., & Schaerer, P. A. (2006). *The avalanche handbook*. Mountaineers Books. https://doi.org/10.5860/choice.31-3797

Mcclymont, A. F., Hayashi, M., Bentley, L. R., Muir, D., & Ernst, E. (2010). Groundwater flow and storage within an alpine meadow-talus complex. *Hydrology and Earth System Sciences*, *14*(6), 859–872. https://doi.org/10.5194/hess-14-859-2010

Milner, A. M., Khamis, K., Battin, T. J., Brittain, J. E., Barrand, N. E., Füreder, L., Cauvy-Fraunié, S., Gíslason, G. M., Jacobsen, D., Hannah, D. M., Hodson, A. J., Hood, E., Lencioni, V., Ólafsson, J. S., Robinson, C. T., Tranter, M., & Brown, L. E. (2017). Glacier shrinkage driving global changes in downstream systems. *Proceedings of the National Academy of Sciences of the United States of America*, *114*(37), 9770–9778. https://doi.org/10.1073/pnas.1619807114

Moore, R. D., Pelto, B., Menounos, B., & Hutchinson, D. (2020). Detecting the effects of sustained glacier wastage on streamflow in variably glacierized catchments. *Frontiers in Earth Science*, *8*, 136. https://doi.org/10.3389/feart.2020.00136

Muir, D. L., Hayashi, M., & Mcclymont, A. F. (2011). Hydrological storage and transmission characteristics of an alpine talus. *Hydrological Processes*, *25*(19), 2954–2966. https://doi.org/10.1002/hyp.8060

Munro, D. S. (1989). Surface roughness and bulk heat transfer on a alacier: Comparison with eddy correlation. *Journal of Glaciology*, *35*(121), 343–348. https://doi.org/10.3189/S0022143000009266

Munro, D. S. (2004). Revisiting bulk heat transfer on Peyto Glacier, Alberta, Canada, in light of the OG parameterization. *Journal of Glaciology*, *50*(171), 590–600. https://doi.org/10.3189/172756504781829819

Munro, D. S. (2011). Delays of supraglacial runoff from differently defined microbasin areas on the Peyto Glacier. *Hydrological Processes*, *25*, 2983–2994. https://doi.org/10.1002/hyp.8124

Munro, D. S. (2013). Creating a runoff record for an ungauged basin: Peyto Glacier, 2002-2007. In J. W. Pomeroy, C. Spence, & P. H. Whitfield, (Eds.), *Putting prediction in ungauged basins into practice* (pp. 197–204). Canadian Water Resources Association. [online]. http://cwra.org/en/resourcecenter/publications/bookstore/20-publications/245-putting-prediction-in-ungauged-basins-into-practice

Nash, J. E., & Sutcliffe, J. V. (1970). River flow forecasting through conceptual models part I — A discussion of principles. *Journal of Hydrology*, *10*(3), 282–290. https://doi.org/10.1016/0022-1694(70)90255-6

Naz, B. S., Frans, C., Clarke, G., Burns, P., & Lettenmaier, D. P. (2014). Modeling the effect of glacier recession on streamflow response using a coupled glacio-hydrological model. *Hydrology and Earth System Sciences*, *18*, 787–802. https://doi.org/10.5194/hess-18-787-2014

Nienow, P., Sharp, M., & Willis, I. (1998). Seasonal changes in the morphology of the subglacial drainage system, Haut Glacier d'Arolla, Switzerland. *Earth Surface Processes and Landforms*, *23*, 825–843. https://doi.org/10.1002/(SICI)1096-9837(199809)23:9<825::AID-ESP893>3.0.CO;2-2

Ommanney, C. S. L. (2002). Glaciers of the Canadian Rockies. In R. S. Williams & J. G. Ferrigno (Eds.), *Satellite image atlas of the glaciers of the world — North America* (pp. J199–J289). U.S. Geological Survey Professional Paper 1386-J-1.

Østrem, G., Arnold, K., & Ostrem, G. (1970). Ice-cored moraines in southern British Columbia and Alberta, Canada. *Geografiska Annaler. Series A, Physical Geography*, *52*(2), 120. https://doi.org/10.2307/520605

Pellicciotti, F., Buergi, C., Immerzeel, W. W., Konz, M., & Shrestha, A. B. (2012). Challenges and uncertainties in hydrological modeling of remote Hindu Kush–Karakoram–Himalayan (HKH) basins: Suggestions for calibration strategies. *Mountain Research and Development*, *32*(1), 39–50. https://doi.org/10.1659/MRD-JOURNAL-D-11-00092.1

Pepin, N. C., Arnone, E., Gobiet, A., Haslinger, K., Kotlarski, S., Notarnicola, C., Palazzi, E., Seibert, P., Serafin, S., Schöner, W., Terzago, S., Thornton, J. M., Vuille, M., & Adler, C. (2022). Climate changes and their elevational patterns in the mountains of the world. *Reviews of Geophysics*, *60*(1), 1–40. https://doi.org/10.1029/2020rg000730

Pomeroy, J. W., Fang, X., Shook, K., & Whitfield, P. H. (2013). Predicting in ungauged basins using physical principles obtained using the deductive, inductive, and abductive reasoning approach. In J. W. Pomeroy, C. Spence, & P. H. Whitfield, (Eds.), *Putting predictions in ungauged basins into practice* (pp. 41–62). Canadian Water Resources Association. [online]. Available from: http://cwra.org/en/resourcecenter/publications/bookstore/20-publications/245-putting-prediction-in-ungauged-basins-into-practice

Pomeroy, J. W., Gray, D. M., Brown, T., Hedstrom, N. R., Quinton, W. L., Granger, R. J., & Carey, S. K. (2007). The cold regions hydrological model: A platform for basing process representation and model structure on physical evidence. *Hydrological Processes*, *21*(19), 2650–2667. https://doi.org/10.1002/hyp.6787

Pomeroy, J. W., Gray, D. M. M., Landline, P. G., & Landine, P. G. (1993). The prairie blowing snow model: Characteristics, validation, operation. *Journal of Hydrology*, *144*(1–4), 165–192. https://doi.org/10.1016/0022-1694(93)90171-5

Pomeroy, J. W., & Li, L. (2000). Prairie and arctic areal snow cover mass balance using a blowing snow model. *Journal of Geophysical Research: Atmospheres*, *105*(D21), 26619–26634. https://doi.org/10.1029/2000JD900149

Pomeroy, J. W., Marsh, P., & Gray, D. M. (1997). Application of a distributed blowing snow model to the Arctic. *Hydrological Processes*, *11*(11), 1451–1464. https://doi.org/10.1002/(SICI)1099-1085(199709)11:11<1451::AID-HYP449>3.0.CO;2-Q

Pradhananga, D., & Pomeroy, J. W. (2022a). Recent hydrological response of glaciers in the Canadian Rockies to changing climate and glacier configuration. *Hydrology and Earth System Sciences*, *26*, 2605–2616. https://doi.org/10.5194/hess-26-2605-2022

Pradhananga, D., & Pomeroy, J. W. (2022b). Diagnosing changes in glacier hydrology from physical principles using a hydrological model with snow redistribution, sublimation, firnification and energy balance ablation algorithms. *Journal of Hydrology*, *608*, 127545. https://doi.org/10.1016/j.jhydrol.2022.127545

Pradhananga, D., Pomeroy, J. W., Aubry-Wake, C., Munro, D. S., Shea, J., Demuth, M. N., Kirat, N. H., Menounos, B., & Mukherjee, K. (2021). Hydrometeorological, glaciological and geospatial research data from the Peyto Glacier Research Basin in the Canadian Rockies. *Earth System Science Data*, *13*(6), 2875–2894. https://doi.org/10.5194/essd-13-2875-2021

Radic, V., & Hock, R. (2014). Glaciers in the Earth's hydrological cycle: Assessments of glacier mass and runoff changes on global and regional scales. *Surveys in Geophysics*, *35*(3), 813–837. https://doi.org/10.1007/s10712-013-9262-y

Ragettli, S., Immerzeel, W. W., & Pellicciotti, F. (2016). Contrasting climate change impact on river flows from high-altitude catchments in the Himalayan and Andes Mountains. *Proceedings of the National Academy of Sciences*, *113*(33), 9222–9227. https://doi.org/10.1073/pnas.1606526113

Rasouli, K., Pomeroy, J. W., Janowicz, J. R., Carey, S. K., & Williams, T. J. (2014). Hydrological sensitivity of a northern mountain basin to climate change. *Hydrological Processes*, *28*(14), 4191–4208. https://doi.org/10.1002/hyp.10244

Reid, T., & Brock, B. W. (2010). An energy-balance model for debris-covered glaciers including heat conduction through the debris layer. *Journal of Glaciology*, *56*(199), 903–916. https://doi.org/10.3189/002214310794457218

Saberi, L., Mclaughlin, R. T., Ng, G.-H. C., Frenierre, J. L., Wickert, A. D., Baraer, M., Zhi, W., Li, L., & Mark, B. G. (2019). Multi-scale temporal variability in meltwater contributions in a tropical glacierized watershed. *Hydrology and Earth System Sciences*, *23*, 405–425. https://doi.org/10.5194/hess-23-405-2019

Schaefli, B., & Gupta, H. V. (2007). Do Nash values have value? *Hydrological Processes*, *21*, 2075–2080. https://doi.org/10.1002/hyp

Schaefli, B., Hingray, B., Niggli, M., & Musy, A. (2005). A conceptual glacio-hydrological model for high mountainous catchments. *Hydrology and Earth System Sciences*, *9*, 95–109. https://doi.org/10.5194/hessd-2-73-2005

Schaefli, B., & Huss, M. (2011). Integrating point glacier mass balance observations into hydrologic model identification. *Hydrology and Earth System Sciences*, *15*(4), 1227–1241. https://doi.org/10.5194/hess-15-1227-2011

Schweizer, J., Kronholm, K., Jamieson, B., & Birkeland, K. W. (2008). Review of spatial variability of snowpack properties and its importance for avalanche formation. *Cold Regions Science and Technology*, *51*(2–3), 253–272. https://doi.org/10.1016/J.COLDREGIONS.2007.04.009

Seibert, J., Vis, M., Lewis, E., & van Meerveld, H. J. (2018). Upper and lower benchmarks in hydrological modelling. *Hydrological Processes*, *32*, 1120–1125. https://doi.org/10.1002/hyp.11476

Sen, P. K. (1968). Estimates of the regression coefficient based on Kendall's Tau. *Journal of the American Statistical Association*, *63*(324), 1379–1389. https://doi.org/10.1080/01621459.1968.10480934

Seneviratne, S. I., Nicholls, N., Easterling, D., Goodess, C. M., Kanae, S., Kossin, J., Luo, Y., Marengo, J., McInnes, K., Rahimi, M., Reichstein, M., Sorteberg, A., Vera, C., Zhang, X., Rusticucci, M., Semenov, V., Alexander, L. V., Allen, S., Benito, G., … Zwiers, F. W. (2012). Changes in climate extremes and their impacts on the natural physical environment. In *Managing the risks of extreme events and disasters to advance climate change adaptation*. Cambridge University Press.

Sentlinger, G., Fraser, J. & Baddock, E. (2019). Salt dilution flow measurement: Automation and uncertainty. In *HydroSenSoft, international symposium and exhibition on hydro-environment sensors and software*. Madrid, 8. Available at: http://www.fathomscientific.com/wp-content/uploads/2018/12/HydroSense_AutoSalt_2019_V0.6.pdf

Shannon, S., Smith, R., Wiltshire, A., Payne, T., Huss, M., Betts, R., Caesar, J., Koutroulis, A., Jones, D., & Harrison, S. (2019). Global glacier volume projections under high-end climate change scenarios. *The Cryosphere*, *13*(1), 325–350. https://doi.org/10.5194/TC-13-325-2019

Shea, J. M., Immerzeel, W. W., Wagnon, P., Vincent, C., & Bajracharya, S. (2015). Modelling glacier change in the Everest region, Nepal Himalaya. *The Cryosphere*, *9*(3), 1105–1128. https://doi.org/10.5194/tc-9-1105-2015

Stahl, K., & Moore, R. D. (2006). Influence of watershed glacier coverage on summer streamflow in British Columbia, Canada. *Water Resources Research*, *42*(6), 1–5. https://doi.org/10.1029/2006WR005022

Stahl, K., Moore, R. D., Shea, J. M., Hutchinson, D., & Cannon, A. J. (2008). Coupled modelling of glacier and streamflow response to future climate scenarios. *Water Resources Research*, *44*(2), 1–13. https://doi.org/10.1029/2007WR005956

Van Loon, A. F., Ploum, S. W., Parajka, J., Fleig, A. K., Garnier, E., Laaha, G., & Van Lanen, H. A. J. (2015). Hydrological drought types in cold climates: Quantitative analysis of causing factors and qualitative survey of impacts. *Hydrology and Earth System Sciences*, *19*(4), 1993–2016. https://doi.org/10.5194/hess-19-1993-2015

van Tiel, M., Kohn, I., Van Loon, A. F., & Stahl, K. (2020). The compensating effect of glaciers: Characterizing the relation between interannual streamflow variability and glacier cover. *Hydrological Processes*, *34*(3), 553–568. https://doi.org/10.1002/hyp.13603

van Tiel, M., Stahl, K., Freudiger, D., & Seibert, J. (2020). Glacio-hydrological model calibration and evaluation. *Wiley Interdisciplinary Reviews: Water*, *7*(6), 1-51. https://doi.org/10.1002/wat2.1483

van Tiel, M., Van Loon, A. F., Seibert, J., & Stahl, K. (2021). Hydrological response to warm and dry weather: Do glaciers compensate? *Hydrology and Earth System Sciences*, *25*(6), 3245–3265. https://doi.org/10.5194/hess-25-3245-2021

Verbunt, M., Gurtz, J., Jasper, K., Lang, H., Warmerdam, P., & Zappa, M. (2003). The hydrological role of snow and glaciers in alpine river basins and their distributed modeling. *Journal of Hydrology*, *282*(1–4), 36–55. https://doi.org/10.1016/S0022-1694(03)00251-8

Walmsley, J. L., Taylor, P. A., & Keith, T. (1986). A simple model of neutrally stratified boundary-layer flow over complex terrain with surface roughness modulations (MS3DJH/3R). *Boundary-Layer Meteorology*, *36*(1–2), 157–186. https://doi.org/10.1007/BF00117466

Wheater, H. S., Pomeroy, J. W., Pietroniro, A., Davison, B., Elshamy, M., Yassin, F., Rokaya, P., Fayad, A., Tesemma, Z., Princz, D., Loukili, Y., DeBeer, C. M., Ireson, A. M., Razavi, S., Lindenschmidt, K. E., Elshorbagy, A., MacDonald, M., Abdelhamed, M., Haghnegahdar, A., & Bahrami, A. (2022). Advances in modelling large river basins in cold regions with Modélisation Environmentale Communautaire—Surface and Hydrology (MESH), the Canadian hydrological land surface scheme. *Hydrological Processes*, *36*(4), e14557. https://doi.org/10.1002/HYP.14557

WMO. (1986). *Intercomparison of models of snowmelt runoff (Operational Hydrology Report No. 23)*. Secretariat of the World Meteorological Organization.

Young, G. J. (1977). Relations between mass-balance and meteorological variables. *Zeitschrift für Gletscherkunde und Glazialgeologie*, *13*(1/2), 111–125.

Zhou, J., Pomeroy, J. W., Zhang, W., Cheng, G., Wang, G., & Chen, C. (2014). Simulating cold regions hydrological processes using a modular model in the west of China. *Journal of Hydrology*, *509*, 13–24. https://doi.org/10.1016/J.JHYDROL.2013.11.013

How to cite this article: Aubry-Wake, C., Pradhananga, D., & Pomeroy, J. W. (2022). Hydrological process controls on streamflow variability in a glacierized headwater basin. *Hydrological Processes*, *36*(10), e14731. https://doi.org/10.1002/hyp.14731

APPENDIX A

TABLE A1 Geomorphic characteristics of the CRHM hydrological response units (HRUs). The HRU number are found on Figure 1b. The cover-type refer to the landscape at the beginning of the simulation, and the land cover type in parenthesis refer to the landscape in 2015.

HRU number	Elevation (m)	Area (km^2)	Slope (°)	Aspect (°)	Cover type
1	2949	0.3231	29.53	40	Glacier
2	2802	1.786	15.91	40	Glacier
3	2701	0.2819	5.203	344	Glacier
4	2654	0.8719	12.33	344	Glacier
5	2560	1.459	14.05	3	Glacier
6	2449	0.8744	8.181	352	Glacier
7	2252	0.3325	7.438	27	Glacier
8	2211	0.2331	4.749	350	Glacier (Moraine)
9	2176	0.2971	6.566	350	Glacier (Moraine)
10	2141	0.0863	13.96	307	Moraine
11	2956	0.2594	29.35	67	Glacier
12	2799	1.104	15.19	67	Glacier
13	2660	0.9737	15.33	60	Glacier
14	2552	0.3394	12.98	40	Glacier
15	2460	0.2731	10.9	75	Glacier
16	2405	0.2081	10.4	72	Glacier (Steep talus)
17	2251	0.0719	10.68	15	Debris-cover
18	2705	0.5981	20.14	84	Glacier
19	2545	0.3425	14.01	121	Glacier
20	2445	0.2275	10.06	111	Glacier (Moraine)
21	2200	0.1306	7.914	40	Debris-cover (Moraine)
22	2741	0.965	26.63	184	Steep talus
23	2501	0.7519	16.57	180	Moraine
24	2554	0.6163	43.62	103	Cliff
25	2273	0.4619	19.19	118	Ice-cored moraine
26	2215	0.26	14.16	145	Moraine
27	2771	1.395	27.97	250	Steep talus
28	2502	0.5512	13.54	256	Moraine
29	2285	0.4463	25.06	305	Ice-cored moraine
30	2702	0.4806	44.91	326	Cliff
31	2533	0.4644	26.58	287	Moraine
32	2375	0.9269	18.38	278	Moraine
33	2393	0.1144	8.185	33	Debris-cover
34	2413	0.1912	7.622	7	Glacier
35	2482	0.09313	24.17	70	Cliff
36	2727	0.35	30.54	80	Cliff
37	2847	0.2625	38.12	4	Cliff

APPENDIX B

Glacier melt contributions to streamflow are divided between melt and wastage following Comeau et al. (2009), with wastage corresponding to net glacier volume loss resulting from negative mass balance and melt referring to a storage term from snowfall and snowmelt. A key difference is the inclusion of the firn melt component to the glacier ice melt calculations.

In years of positive or neutral mass balance, the glacier ice and firn melt is lower than the leftover snowfall at the end of the melt season, and no wastage occurs. During these years, the melt component equals to the ice melt M_i.

$$M_i + M_f \leq P_s - M_s, \text{Wastage} = 0, \text{Melt} = M_i$$

Where M_i is the glacier ice melt, M_f is the glacier firn melt, P_s is the snowfall over the glacier area, and M_s is the snowmelt over the glacier area.

In years with negative mass balance, the ice and firn melt from the glacier area is larger than the residual snowfall at the end of the melt season:

$$M_i + M_f > P_s - M_s$$

$$\text{Wastage} = (M_i + M_f) - (P_s - M_s)$$

$$\text{Melt} = P_s - M_s$$

In years of negative mass balance, wastage is defined as the volume of ice and firn melt that exceeds the water equivalent volume of snow accumulation into the glacier.

The percentage of glacier wastage contribution to streamflow is calculated as a percentage of the annual basin yield, defined as the combination of streamflow simulated at the basin outlet and groundwater discharge from the basin.

The individual components of the wastage calculation are shown in Figure B1. In the case of Peyto, due to both rain-on-snow events and snow redistribution from blowing snow and avalanches, the glacier area snowmelt (M_s) is slightly larger than the glacier area snowfall (P_s) for 21 out of the 32 years analysed. In these 21 years, the snowmelt is on average 10% higher than the snowfall across the glacier, with a maximum difference of 27%.

Of the 32 years simulated, only 2 years do not have a wastage component, due to showing a positive mass balance with the ice melt component being smaller or equal to the snow remaining on the glacier at the end of the hydrological year (P_s – M_s). For the 30 years with wastage, the wastage volume was calculated as a ratio to the total basin yield (combined streamflow and groundwater), and contributed between 6% and 77% of basin yield, and averaging 53%.

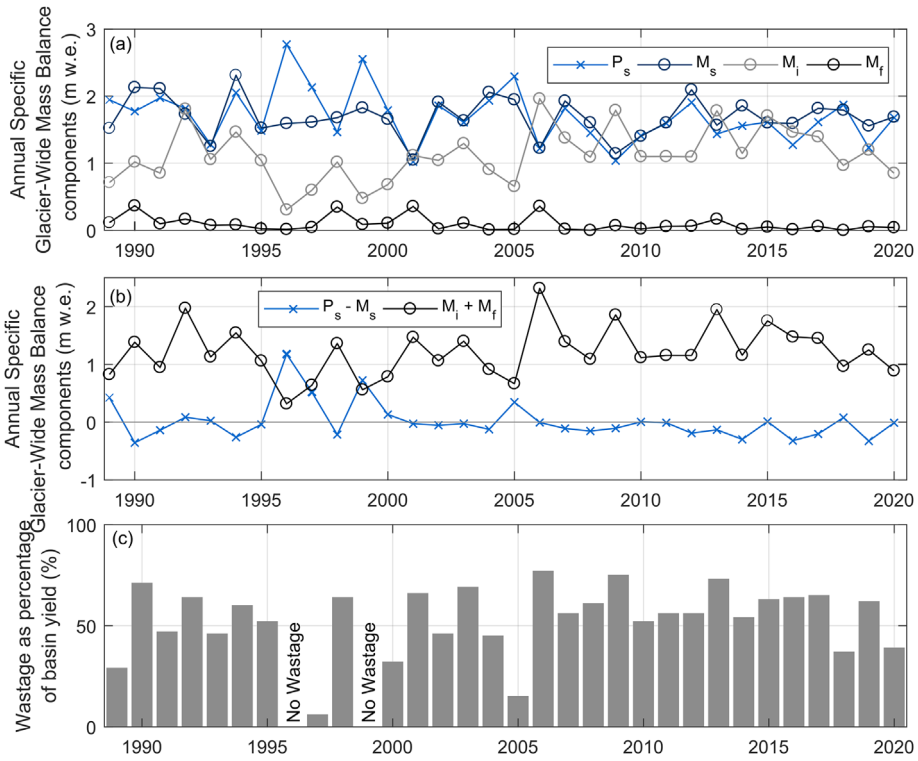

FIGURE B1 Annual specific mass-balance components for the Peyto Glacier for years 1988–2020, with annual snowfall (P_s), snow melt (M_s), ice melt (M_i) and firn melt (M_f) in (a), the combined snow components (P_s – M_s) and glacier ice and firn (M_i + M_f) in (b) and the wastage as a proportion of annual basin yield in (c).